Molecular Dynamics Simulation of a Bilayer of 200 Lipids in the Gel and in the Liquid Crystal Phase[‡]

Helmut Heller[§] Michael Schaefer[¶]
Klaus Schulten[*]

Beckman Institute and Department of Physics
University of Illinois
405 N. Mathews Avenue, Urbana, IL 61801 U.S.A.

Running title: Simulation of a membrane–water system.

Key words: phosphatidylcholine, lipid membrane, stochastic boundary, liquid crystal phase

[‡]This work was supported by the National Institutes of Health Resource "Concurrent Biological Computing" under grant number 1 P41 RR05969*01. M.S. was partially supported by a NATO postdoctoral fellowship.

[§]Present address: Ludwig Maximilians University, Institute for Medical Optics, Theresienstr. 37, W-8000 Munich 2, Germany; e-mail: heller@lisboa.ks.uiuc.edu

[¶]Present address: Harvard University, Department of Chemistry, Cambridge, MA 02138, U.S.A.

[*]To whom correspondence should be addressed.

Abstract

We have constructed and simulated a membrane-water system which consists of 200 molecules of 1-palmitoyl-2-oleoyl-*sn*-glycero-3-phosphatidylcholine forming a rectangular patch of a bilayer and of 5483 water molecules covering the headgroups on each side of the bilayer. The total number of atoms is approximately 27,000. The lateral dimensions of the bilayer are 85 Å×100 Å, and the distance between the bilayer surfaces as given by the average phosphorus to phosphorus distance is 35 Å. The thickness of each water layer is up to 15 Å. In all, we simulated 263 ps of the dynamics of the system. To prevent system disintegration, atoms within 5 Å from the surface were harmonically restrained and treated by Langevin dynamics, forming a stochastic boundary. Interior lipids and water molecules were unrestrained. The first 120 ps of the dynamics calculation were used to equilibrate the system and to achieve a low internal pressure. We performed two simulations for analysis, simulation I of the system that resulted from the equilibration, simulation II of the system after an increase of the area per headgroup from 46 Å^2 to 70 Å^2. The decrease of the lateral lipid density was achieved by scaling the atomic x, y and z-coordinates independently, leaving the volume of the system constant. For both simulations I and II, we determined the internal pressure, the lipid self-diffusion coefficients, the order parameter profile, the distribution of molecular groups, and other properties. The parameters extracted from simulation II are in good agreement with observations on bilayers in the liquid-crystal phase. We provide evidence that the bilayer of simulation I corresponds to the gel phase. The membrane structures resulting from this work can be used for molecular dynamics investigations of membrane proteins, e. g., for the study of lipid-protein interactions or for the equilibration of structural models.

Membrane proteins and membrane related processes have been the subject of experimental [2, 3, 4, 5] and theoretical [6, 7, 8, 9, 10, 11] research during the past forty years. The interest of the theoretical community in investigating biological membranes has been relatively low. One reason may have been the fact that only very little structural information on membranes and on membrane proteins exists. Another reason might be the statistical nature of lipid membrane structures which requires either large systems and/or long time ranges for proper characterizations. Also, because of limitations in computer power researchers until recently were generally restricted to molecular dynamics studies of biopolymer systems entailing only a few thousand atoms [12, 13, 14, 15], which is too few to encompass membranes and membrane-protein systems. There is evidence, however, that the environment has a strong influence on the structure and function of proteins, both in solution and in membranes [16, 17, 18, 19, 11] and, hence, a study of membranes with and without proteins is most desirable.

Early theoretical investigations of membranes were carried out by Marčelja [6], who introduced a molecular field model to represent the influence of neighboring lipid molecules. One drawback of this approach is that it cannot reproduce cooperative effects of several lipid molecules. As computers became more powerful, MD[1] simulations of small lipid systems (2 x 16 decanoate molecules) over short times of the order of 100 ps became feasible [20]. Periodic boundary conditions together with the small system size gave rise to artifacts which were reduced in later studies by increasing the system size to 2 x 64 decane molecules [21]. Simulation of *complete* lipid molecules (2 x 24 DMPE molecules and 553 water molecules [22]) made the model more realistic. Another improvement was the inclusion of water and ions in the simulation [23]. In addition to monolayers and bilayers, micelle-water systems have also been simulated [24, 25].

The time range of the simulations listed above is of the order of 100 ps. Such a short time range prevents the investigation of many membrane properties, e.g., of phase transitions, which occur on time scales in the range of microseconds and longer. A combination of Brownian dynamics with the Marčelja molecular field model allowed the simulation of a single chain of a DPPC molecule for $0.66\,\mu$s [26, 27]. Here too, the simulations were improved by increasing the size of the system to as much as 84 molecules [10, 28].

One very promising outcome of simulations of biological membranes is use of the simulated systems in investigations of membrane-protein interactions [16]. With the advent of modern supercomputers, especially of parallel machines providing computing power in the GFLOPS range [29, 30], and with the development of efficient algorithms for the evaluation of long-range Coulomb forces [31, 32, 33, 34, 1, 35], the study of large and heterogeneous systems using molecular dynamics has become increasingly feasible. In this article, we report on molecular dynamics simulations on a self-built parallel computer [29] of a $85\,\text{Å}\times 100\,\text{Å}$ patch of membrane bilayer covered with up to 15 Å of water on each side. The system was specifically

[1]Abbreviations: MD, molecular dynamics; MIMD, multiple instructions, multiple data; GFLOPS, Giga FLoating Point Operations Per Second; DRAM, dynamic random access memory; POPC, 1-palmitoyl-2-oleoyl-*sn*-glycero-3-phosphatidylcholine; DPPC, 1,2-dipalmitoyl-*sn*-glycero-3-phosphatidylcholine; DOPC, 1,2-dioleoyl-*sn*-glycero-3-phosphatidylcholine; DMPC, 1,2-dimyristoyl-*sn*-glycero-3-phosphatidylcholine; DMPE, 1,2-dimyristoyl-*sn*-glycero-3-phosphatidylethanolamine; DLPE, 1,2-dilauroyl-*sn*-glycero-3-phosphatidylethanolamine.

chosen large enough to accommodate a membrane protein of about 20,000 molecular weight, e.g., bacteriorhodopsin, and for the purpose of embedding larger proteins it can easily be enlarged. Another objective of this work was to ensure that the simulated bilayer is in the liquid-crystal phase (L_α) which is the biologically most relevant membrane phase [36]. From experiments, it is known that POPC is in the liquid-crystal phase in a wide temperature range from -5^o C to 70^o C [37]. Other important membrane phases are the crystal phase (L_c) and the gel phase ($L_{\beta'}$) [38].

In the following section, we describe the construction of a starting configuration of the bilayer, the methods used for simulating the system, for changing the system setup and for analyzing the trajectories. In the Results section, we report on five molecular dynamics calculations, termed Equilibration, Simulation I, "Disaster I" and "Disaster II", and Simulation II. During Equilibration, special emphasis was put on investigating and adjusting the pressure in the system which involved a series of changes of the stochastic boundary setup. The simulation conditions were invariant during Simulation I and II which were calculated for detailed analysis. The initial structure of Simulation II was generated from the final structure of Simulation I by increasing the lateral area of the bilayer by 50%. The simulations "Disaster I" and "Disaster II" are two unsuccessful attempts at inducing such an increase. The alteration in the simulation conditions in going from Simulation I to Simulation II successfully induced a phase change in the bilayer from the gel phase ($L_{\beta'}$) to the liquid-crystal phase (L_α).

Methods

Parallel Computation

For the molecular dynamics simulations reported in this article, we employed a 60 node MIMD type parallel computer with double ring architecture which was built in our research group [29, 39]. Each node of this machine consists of a T800 Transputer processor with 4 MByte DRAM. The computer achieves Cray 2 processor speed for molecular dynamics calculations [40, 41]. The total computer time for all the simulations described in this paper amounts to more than 14,640 hours or 20 months of continuous runtime.

We used the molecular dynamics program EGO [42, 29, 43, 41]. EGO is written in occam II and achieves a speed proportional to the number of nodes. The program is input/output-compatible with CHARMm [44] and X-PLOR [45, 46]. EGO employs the CHARMm force field and can be started using X-PLOR restart files. The program uses a modified Verlet algorithm [47] with a distance class algorithm [1] for the non-bonded interactions, i.e., it does not truncate the Coulomb and van der Waals forces[2]. With respect to the electrostatic interaction, the distance class algorithm is an alternative to the fast multipole algorithm [33]. A parallel version of the SHAKE algorithm [48, 49] constrains the bond length for hydrogen atoms and allows an integration time step of 1 fs. For the analysis of the simulation data, we used X-PLOR [46] as well as software developed by the authors.

[2] A paper which focusses on the consequences of cut-off in membrane simulations is currently in preparation.

Construction of the Membrane Bilayer

We chose POPC as the lipid for the construction of the bilayer, because it is one of the most prevailing phospholipids. POPC has one saturated palmitoyl and one unsaturated oleoyl fatty acid tail. The presence of one unsaturated hydrocarbon tail enables one to study effects of unsaturation. The lipid can be easily altered to DPPC, probably the most widely studied phospholipid.

We constructed one POPC molecule using the program *ChemNote* within the molecular graphics package *Quanta* [50]. Hydrogen atoms were represented by compound atoms. The chemical structure of POPC is given in Fig. 1. In the initial structure of this molecule all

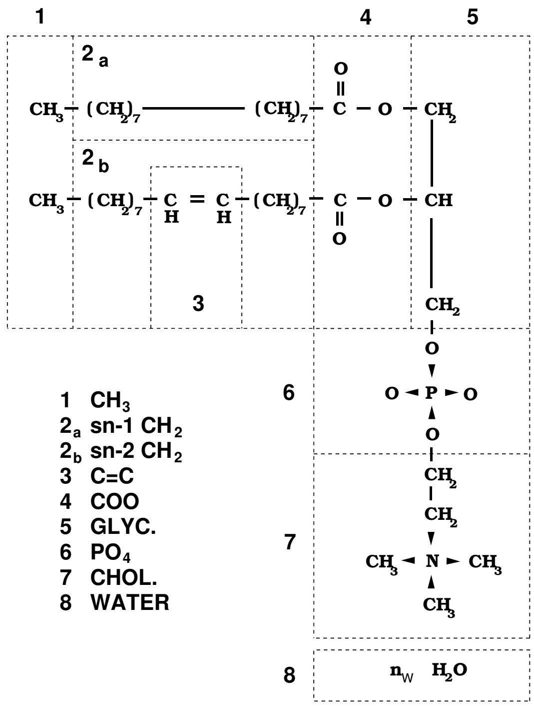

Figure 1: Chemical structure of POPC and the classification of lipid and water atoms into eight groups. The classification is referred to by the cross-membrane profiles, below, and is analogous to the parsing of DOPC in [51].

dihedrals of the tails and head group were in the *trans* form, exept for the C=C double bond which was in the *cis* form.

With interactive graphics, we arranged the lipid in an extended "upright" configuration, with both hydrocarbon tails and the head group pointing along the y-axis, which was to become the bilayer normal. After 100 steps of steepest descent minimization within *Quanta*, four identical copies of the molecule were arranged in a staggered configuration, forming the building block for the monolayer (see Fig. 2). After another minimization of 200 steps, we calculated a 1 ps molecular dynamics trajectory applying velocity rescaling in order to reduce the energy content of the building block. At first, the system spontaneously heated up to a temperature of 600 K, but within the simulation time of 1 ps, it reached the target

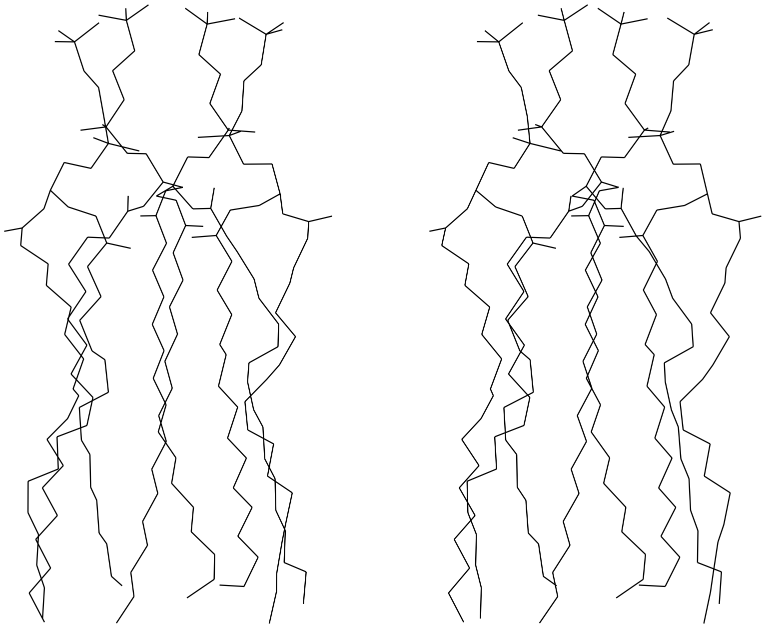

Figure 2: Stereo diagram of the building block of four lipids (left: left eye view; right: right eye view). The lipids are arranged in a staggered configuration such that the tail of one lipid reaches into the void between the two tails of another lipid.

temperature of 300 K. The preparation of the building block was then completed by another 100 steps of steepest descent minimization. Subsequently, 25 building blocks were arranged in a 5×5 grid to form one layer of the membrane, which was minimized for 100 steps. This layer was duplicated, rotated and shifted to obtain a bilayer, leaving a 1 Å distance between the maximum y-coordinate of atoms in the lower layer and the minimum y-coordinate of atoms in the upper layer. We obtained a membrane patch with a lateral area of 68 Å×80 Å and a thickness of 44 Å, the latter referring to the average phosphorus to phosphorus distance between the monolayers.

To complete the construction, the two membrane surfaces were covered by up to 15 Å of water (see Fig. 3) which corresponds to approximately six layers of water molecules. Additional water molecules were placed in the head group region to fill available space. The initial positions of the water oxygen atoms were on a hexagonal lattice with a unit cell size corresponding to the density of water at normal conditions. The orientation of the hexagonal lattice as well as the orientation of each water molecule was chosen at random. The resulting initial system consisted of 200 lipid molecules and 4,526 water molecules with the total number of atoms equal to 23,978.

To equilibrate the system, we computed a trajectory of more than 120 ps. For the lipid molecules, we used the atom type assignments and the partial charge set provided by *ChemNote* within *Quanta*. The bonded and van der Waals potential parameters were taken from

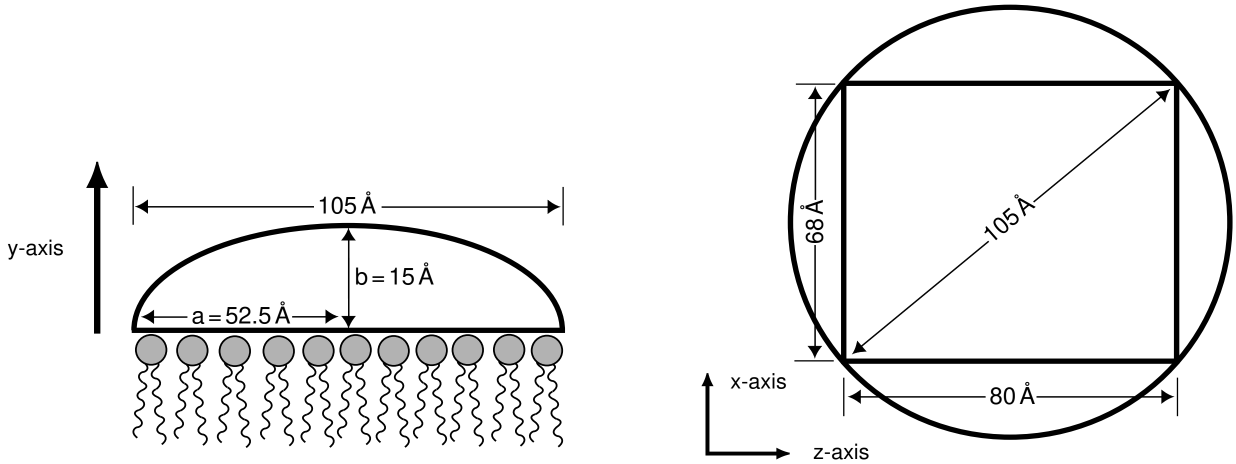

Figure 3: Schematic diagram of one watercap in the initial membrane geometry used during Equilibration, Simulation I, "Disaster I" and "Disaster II". For each water molecule, the distance d from the bilayer surface satisfies $d(x, z) \leq \sqrt{b^2 - b^2(x^2 + z^2)/a^2}$, where $2a$ is the diagonal of the bilayer surface, $b = 15$ Å the maximum thickness of the water cap, and x, y, z are the coordinates of the water molecule, with the bilayer centered at the origin. The water molecules are therefore located inside an ellipsoid generated by rotation around the bilayer normal. Left: side view of the upper water cap with one diagonal of the bilayer surface in the paper plane. Right: top view; no water molecules were placed outside the rectangular membrane surface.

the parameter file param19.pro of X-PLOR. For the water molecules we employed TIPS3P[3] parameters [52]. After the equilibration, we adopted a dataset[4] provided to us by A. MacKerell of the Department of Chemistry at Harvard [53] for the lipid partial charges. The parameters of the bonded potential and of the van der Waals potential were not changed.

At the begin of Simulation II, we changed the lateral area per lipid molecule such as to agree with experimental data (see the section on coordinate rescaling) and we constructed new watercaps. For simplicity, these watercaps were given a rectangular geometry and the water oxygen atoms were placed initially on a cubic lattice. As with the original water caps, the orientation of the water molecules and of the whole lattice was chosen at random. The thickness of the two water layers was 10 Å which, in conjunction with the increased lateral dimensions of the bilayer of 85 Å×100 Å, led to a total number of 5,483 water molecules. Accordingly, the total number of atoms of the bilayer-water system increased to 26,849.

Stochastic Boundary

A stochastic boundary (Langevin dynamics) [54, 55] with harmonic restraints was used to couple the system to a heat bath and prevent system disintegration. The Langevin dynamics

[3]parameter file param19.sol of X-PLOR

[4]parameter and topology file Charmm22 of CHARMm

algorithm implemented by EGO is as described in [56], and the harmonic restraint energy of an atom is calculated according to $E_{\rm har} = k_{\rm har} \cdot (\vec{P} - \vec{P}_0)^2$, where $\vec{P}$ and $\vec{P}_0$ are the location of the atom and it's reference position. During all simulations reported in this paper, the heat bath temperature, affecting atoms in the stochastic boundary only, was set equal to 300 K.

Friction and stochastic forces were gradually increased from the inside to the outside within a boundary of thickness $\Delta = 8$ Å. During Simulation II, the boundary thickness was reduced to $\Delta = 5$ Å. For an atom at position $\vec{P}$, a switching function $S(\vec{P})$ was used to determine the harmonic force constant of the restraining potential $k_{\rm har}(\vec{P}) = k_{\rm max} \cdot S(\vec{P})$, and the collision frequency $f(\vec{P}) = f_{\rm max} \cdot S(\vec{P})$. For simplicity, we used an atom-type independent maximum collision frequency of $f_{\rm max} = 30$ /ps and a maximum harmonic force constant of $k_{\rm max} = 17.2$ kcal/(mol Å^2), which corresponds to a harmonic oscillation frequency of $\omega = 20$/ps. Hydrogens were not assigned friction or harmonic force constants. The switching function $S(\vec{P})$ is a combination of two switching parameters, one depending on the minimum distance d_{xz} to the lateral boundary and the other depending on the minimum distance d_y to the surface of the water caps

$$S(\vec{P}) = F_{\rm s}(\Delta - d_{xz}) + F_{\rm s}(\Delta - d_y) - \sqrt{F_{\rm s}(\Delta - d_{xz}) \cdot F_{\rm s}(\Delta - d_y)} \quad . \tag{1}$$

Here, $F_{\rm s}$ is the switching function

$$F_{\rm s}(x) = \begin{cases} 0\,, & \text{if } x \leq 0\,; \\ x^2(3\Delta - 2x)/(2\Delta^3)\,, & \text{if } 0 \leq x \leq \Delta\,; \\ 1/2\,, & \text{if } x \geq \Delta\,. \end{cases} \tag{2}$$

During Simulation I, the harmonic restraints on lipid atoms were reduced by a factor of 50 and those on water oxygens by a factor of 5 in order to reduce the rigidity of the boundary. During Simulation II, only the lipid phosphorus atoms and water oxygens were restrained and the maximum harmonic force constant was reduced by a factor of 5. The maximum friction constant was kept at the value given above.

Pressure and Surface Tension

The pressure in the system was determined in two different ways: by evaluating the forces on the boundary atoms from the harmonic restraints (boundary method) and by using the virial method [57]. Because EGO does not provide easy access to the forces and velocities during a dynamics run, we used the virial method only in a few instances to check the pressures which were obtained with the boundary method.

Surface Tension

Since the dimensions of the system described here are very small compared to macroscopic systems, the contribution of the surface tension to the pressure cannot be neglected. Assuming a spherical system with radius R, this contribution is $p_{\rm surf} = -2\sigma/R$, where σ is the surface tension. The negative sign of the pressure reflects the tendency of the surface tension to reduce the size of the system. From the volume of the membrane-water system, one can estimate $R \approx 36.5\,\text{Å}$, while the surface tension at the interface between water and air at 305 K is $\sigma = 0.071\,\text{N/m}$ [58, 59]. We, therefore, have an approximate contribution of $p_{\text{surf}} \approx -39\,\text{MPa}$ to the pressure in the system[5]. These considerations apply to both Equilibration and Simulation I, for which we had chosen a curved outer boundary for the two watercaps, with a radius of curvature in the range from 15 Å to about 60 Å. For a rectangular system, one can derive an expression for the pressure contribution from surface tension that is identical to the one above, with R now the thickness of the bilayer [21]. The difference is that for this geometry, the contribution is to the lateral pressure only.

Boundary Method

The pressures on the six faces of the system were calculated independently. Ignoring the curvature of the two surfaces in the y direction, the total surface is given by six rectangles. To reduce the risk of introducing an error in the pressure calculation related to the edges and corners of the system boundary, we cut off 15Å from the edges of each surface rectangle. Let $\hat{n}$ be the normal vector on a surface rectangle, pointing outward. To calculate the pressure on the surface rectangle, we determined the boundary atoms belonging to it, calculated the negative sum of all restraining forces acting on them, took the scalar product of that force with $\hat{n}$ and divided by the area A of the rectangle:

$$
\begin{aligned}
p(t) &= -\frac{1}{A}\sum_i \vec{F}_i^{\text{har}}(t)\cdot\hat{n} \quad ; &(3)\\
\vec{F}_i^{\text{har}}(t) &= -2\,k_i^{\text{har}}\cdot(\vec{P}_i(t)-\vec{P}_i(0)) \quad . &(4)
\end{aligned}
$$

Here, k_i^{har} is the force constant of the restraining potential (see the section on the stochastic boundary), $\vec{P}_i(t)$ the actual and $\vec{P}_i(0)$ the reference position of atom i. Note that a shift of atom i towards the outside, i.e., $(\vec{P}_i(t)-\vec{P}_i(0))\cdot\hat{n} > 0$, leads to a positive pressure contribution even though the restraining force points inwards.

Virial Method

According to the virial method [57], the pressure of a molecular system is given by

$$
p = \frac{2}{3V}(E_{\text{kin}} - \Xi) \quad , \tag{5}
$$

where Ξ is the internal virial for pair-additive potentials, E_{kin} is the kinetic energy, and V is the volume of the system. Because intra-molecular forces necessarily sum up to zero, the

[5] $1\,\text{MPa} = 10^6\,\text{N/m}^2 = 10\,\text{bar}$

internal virial Ξ is given by

$$\Xi = -\frac{1}{2} \sum_{i<j} (\vec{P}_i^{\mathrm{CM}} - \vec{P}_j^{\mathrm{CM}}) \cdot \vec{F}_{ij} \tag{6}$$

where $\vec{P}_i^{\mathrm{CM}}$ is the location of the center of mass of molecule i and $\vec{F}_{ij}$ is the net force exerted by molecule j on molecule i. Note that only van der Waals and Coulomb interactions contribute to $\vec{F}_{ij}$.

Rescaling of Coordinates and Reference Positions

At various points in our simulation it was necessary to change the size of the system. For this purpose we employed two different schemes, termed atomic rescaling and molecular rescaling. Atomic rescaling was done by multiplying all coordinates by a scaling factor f. We generalized this method by allowing for an independent rescaling of the atomic x, y, and z coordinates with scaling factors f_x, f_y, and f_z, respectively. This non-uniform scaling procedure enabled us to change the shape of the membrane patch, e.g., to reduce the thickness of the bilayer without altering the lateral area. In order to make small adjustments or to shrink the system, we rescaled only the reference positions for the harmonic restraints. When continuing the molecular dynamics simulation, this change would affect only atoms in the boundary which were assigned a non-zero restraining force constant. Due to the harmonic restraint forces, the simulated system gradually adjusted to the altered boundary.

At the beginning of Simulation II, we increased the area per head group by a factor of 1.5 compared to the Equilibration or Simulation I. Such a drastic change could not be accomplished by rescaling of the reference positions, since this caused extremely high restraint energies of the order of 10^5 kcal/mol and very high temperatures during the simulation (see "Disaster II"). Therefore, we changed both the reference positions and the actual coordinates of the atoms.

However, atomic rescaling of the positions inevitably distorts the molecular structure, in particular bond lengths, and, if non-uniform scaling is used, also bond-angles and dihedrals. A rescaling by a factor as large as 1.5 would introduce large, unwanted contributions into the bonded energy and force terms. Therefore, we adopted a method which we termed molecular rescaling. First, the centers of mass $\vec{P}_i^{\mathrm{CM}}$ of all molecules were determined. Every molecule was then shifted as a whole, calculating the shift vector $\vec{s}_i$ of molecule i according to $\vec{s}_i = (f-1)\,\vec{P}_i^{\mathrm{CM}}$. Therefore, the new coordinates of an atom belonging to molecule i were given by $\vec{P}_{\mathrm{new}} = \vec{P}_{\mathrm{old}} + \vec{s}_i$. This procedure was only suitable for an expansion of the system ($f > 1$) since in the case of a contraction, the van der Waals repulsion of close contacts would induce very strong forces. As in the case of the atomic rescaling procedure, we scaled the scaling x, y, and z-coordinates independently.

Distribution of Molecular Groups

To determine the distribution of molecular groups across the membrane, i.e., along the y-axis, we used an area $\mathcal{A}_{xz}(y)$ parallel to the bilayer surface for sampling. To define the dimensions of $\mathcal{A}_{xz}$, we started with the smallest rectangle covering all atomic positions of the membrane patch projected onto the xz plane and then cut off 15 Å from all four sides, thus avoiding sampling over restrained atoms in the lateral boundary. The following procedure allowed us to deduce continuous profiles from our data despite the relatively small number of atoms or molecules involved. First, we assigned to the quantities under consideration, e.g., to all CH_2 units, normalized, three dimensional Gaussian density functions:

$$G_i(\vec{x}) = \frac{1}{\pi^{3/2}\sigma^3} \exp\left(-(\vec{x}-\vec{x}_i)^2/\sigma^2\right) \quad . \tag{7}$$

Here, $\vec{x}_i$ denotes the location of unit i. We typically used a value $\sigma = 1.5$ Å for the width to ensure atomic resolution. The average density $\rho(y)$ as a function of y was then determined by integrating the sum of the density functions G_i over $\mathcal{A}_{xz}(y)$ and dividing by the area of $\mathcal{A}_{xz}$:

$$\rho(y) = \frac{1}{|\mathcal{A}_{xz}|} \sum_i \int\limits_{\mathcal{A}_{xz}(y)} G_i \, d^3x \quad . \tag{8}$$

In this expression, the area of $\mathcal{A}_{xz}$ is denoted by $|\mathcal{A}_{xz}|$. If $\mathcal{A}_{xz}$ extends from $-a$ to $+a$ in the x direction and from $-b$ to $+b$ in the z direction, the contribution of a single unit i at (x_i, y_i, z_i) is

$$\int\limits_{\mathcal{A}_{xz}(y)} G_i \, d^3x = \frac{1}{4\pi^{1/2}\sigma} \exp\left(-\frac{(y_i-y)^2}{\sigma^2}\right) \left[\mathrm{erf}\left(\frac{a+x_i}{\sigma}\right) + \mathrm{erf}\left(\frac{a-x_i}{\sigma}\right)\right] \times$$
$$\times \left[\mathrm{erf}\left(\frac{b+z_i}{\sigma}\right) + \mathrm{erf}\left(\frac{b-z_i}{\sigma}\right)\right] \quad , \tag{9}$$

where $\mathrm{erf}(z)$ denotes the error function.

For averaging distributions calculated at different times along a trajectory, it was necessary to define a zero-point of the y-axis which is insensitive to a translation of the whole system. This was accomplished by shifting the geometric center of the lipids to the origin prior to calculating a distribution. The geometric center was determined by averaging the x, y, and z-coordinates of all lipid atoms in the system.

Area per Head Group

To calculate the average area per lipid head group, we first determined the area A_{xz} of the smallest rectangle covering the lipid atoms projected onto the xz plane. The area per lipid is then given by simply dividing A_{xz} by the number of lipid molecules in one layer, namely by 100. To improve the accuracy, we used a set of 20 rectangles for sampling and averaging. The first sampling area was generated by cutting 10Å off the edges of the lateral covering area referred to above. All rectangles had the origin as center, and their length in the x and in the z direction was decreased by 1Å in going from one rectangle to the next. For each rectangle and for both the upper and the lower layer of the membrane, we determined the number of lipid molecules, represented by their center of mass, within the sampling area and then divided the rectangle area by that number. This procedure provided us with a set of 40 values for the area per head group from which we determined both the average area and the standard deviation.

^{2}H Order Parameter

The deuterium order parameter S_{CD} is a critical source of structural and dynamical information on lipids. It is related to the average orientation of the methylene groups and provides information about the order within the bilayer. The traceless order parameter tensor $\mathbf{S}$ is defined as

$$\mathbf{S}_{ij} = \frac{1}{2} \langle 3 \cos\theta_i \cdot \cos\theta_i - \delta_{ij} \rangle \quad , \tag{10}$$

where θ_i, $i \in \{x, y, z\}$, is the angle between the ith molecular axis and the bilayer normal, and the averaging is done over all lipids in the sample and over the sampling time. In our simulations, only completely unrestrained lipids were considered for averaging. The molecular axes are defined for each saturated carbon atom as follows: x is along the H–H vector, y is the bisectrix of the H-C-H angle, and z is defined as the vector perpendicular to the H-C-H plane [21]. For the unsaturated carbons the definition is slightly different, namely z_k is along the vector from C_{k+1} to C_k (where k is the carbon index), x is perpendicular on the plane defined by the H–C vector and the z_k-axis, and y is perpendicular to the plane defined by x and z_k [60]. The experimentally observed deuterium order parameter S_{CD} can be computed using the relation [23]

$$S_{\mathrm{CD}} = \frac{2}{3}\mathbf{S}_{xx} + \frac{1}{3}\mathbf{S}_{yy} \quad . \tag{11}$$

If the molecular motion is such that isotropic rotation around the molecular z-axis occurs, then $\mathbf{S}_{zz} = -2\mathbf{S}_{xx} = -2\mathbf{S}_{yy}$ and $S_{\mathrm{CD}} = -\frac{1}{2}\mathbf{S}_{zz}$ [20]. $\mathbf{S}_{zz}$ is also sometimes referred to as local $\mathbf{S}_{\mathrm{Chain}}$ or $\mathbf{S}_{\mathrm{mol}}$. The coordinates for the hydrogen atoms, which are not directly available as we employ the united atom model for all hydrocarbon atoms, have to be generated for this computation in the usual way (e.g., by using X-PLOR). For computation of the time-averages, configurations were sampled every 128 fs. Extreme cases of the order parameter are $-S_{\mathrm{CD}} = 0.5$ for the extended all-trans configuration (completely ordered state) where the chain is aligned along the bilayer normal ($\theta_i = 90^o$, $i \in \{x, y\}$) and $-S_{\mathrm{CD}} = 0$ if the hydrocarbon groups do not show any preferred orientation (complete disorder).

Diffusion Constant

The self-diffusion constant D is determined by the long time behavior of the mean square displacement ξ of a molecule. According to continuum diffusion theory, the diffusion constant in d dimensions is defined as [61]

$$D = \frac{1}{2d} \lim_{t\to\infty} \frac{d}{dt} \langle \xi^2(t) \rangle \quad . \tag{12}$$

In our case, the two-dimensional lateral square displacement $\xi^2_{\mathrm{lat}}(t)$ and the one-dimensional transversal square displacement $\xi^2_{\mathrm{tra}}(t)$ are

$$\begin{aligned} \xi^2_{\mathrm{lat}}(t) &= \Big(X^{\mathrm{CM}}(t+t_0) - X^{\mathrm{CM}}(t_0) \Big)^2 + \Big(Z^{\mathrm{CM}}(t+t_0) - Z^{\mathrm{CM}}(t_0) \Big)^2 \\ \xi^2_{\mathrm{tra}}(t) &= \Big(Y^{\mathrm{CM}}(t+t_0) - Y^{\mathrm{CM}}(t_0) \Big)^2 \quad . \end{aligned} \tag{13}$$

Here, X^{CM}, Y^{CM}, and Z^{CM} are the Cartesian coordinates of the center of mass of the lipid and t_0 is a point of reference along the simulated trajectory.

We determined the curves of square lateral and transversal displacements by averaging equations (13) over all completely unrestrained lipid molecules. Let $\mathcal{L}_0$ be the set of the latter molecules. To reduce the statistical error, we introduced a further averaging procedure over the set $\{t_0\}$ of all possible reference times. The curve of the mean squared transversal displacement was then calculated according to

$$\langle \xi^2_{\mathrm{tra}}(t) \rangle = \frac{1}{N_0} \sum_{i \in \mathcal{L}_0} \frac{1}{M_0} \sum_{t_j \in \{t_0\}} (Y_i^{\mathrm{CM}}(t+t_j) - Y_i^{\mathrm{CM}}(t_j))^2 \quad . \tag{14}$$

Here, N_0 and M_0 are the number of unrestrained lipids and the number of reference times, respectively. The same averaging was applied to the lateral displacement. The lateral and transversal diffusion constants were then determined from the asymptotic slopes of the corresponding $\xi^2(t)$ curves for "longer" times, formally for $t \to \infty$, in accordance with equation (12).

Obviously, the average transversal displacement $\langle \xi^2_{\mathrm{tra}}(t) \rangle$ must approach a constant value in the limit $t \to \infty$ if the bilayer is not to disintegrate, which means that the long time transversal diffusion constant must vanish in the present case. However, for a time domain in the range of a few ps, the average transversal displacement curve can be expected to have a non-vanishing slope resulting from diffusion within a potential well that is preventing the lipids from leaving a monolayer. With a system of limited size, similar considerations hold true for the lateral diffusion and displacement. In the present study, however, the considerable lateral dimension of the bilayer of $85\times 100\,\text{Å}^2$ justifies the assumption that finite size effects on the lateral displacement can be neglected within a 100 ps time frame.

Results

Equilibration and Volume Adjustment

After the construction, we performed a 120 ps simulation of the membrane-water system in order to equilibrate the assembly and to achieve a low internal pressure that was in agreement with the estimates made for pressure due to surface tension (see Methods). The non-bonded energies, total energy, and temperature of the bilayer during the equilibration are shown in Fig. 4. The pressure on the two watercaps as determined by the boundary method is given in Fig. 5.

Energies

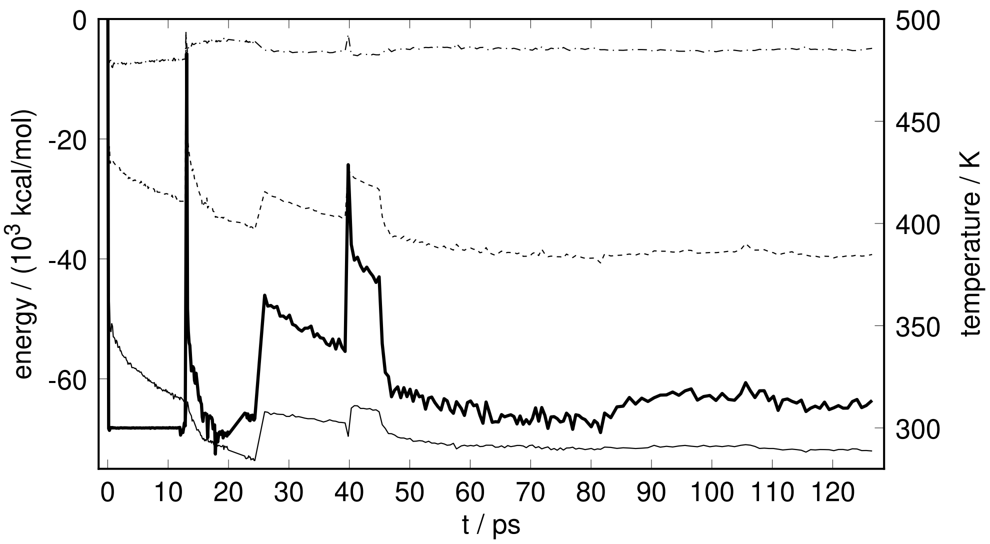

Figure 4: Energies and temperature during the Equilibration simulation: total energy (- - -), Coulomb energy (—), van der Waals energy (–·–·–), and temperature (**—**). During the initial 0.01 ps, the energies and temperature reached maximum values of $E_{\mathrm{tot}} = 8.0 \cdot 10^3$ kcal/mol, $E_{\mathrm{vdW}} = 3.1 \cdot 10^3$ kcal/mol, $E_{\mathrm{Coul}} = -45.4 \cdot 10^3$ kcal/mol and $T = 559$ K (some peaks outside plot range), as a result of the high potential energy of the original setup. The other peaks in the energy and temperature curves resulted from rescaling of the reference positions, i.e., from the corresponding addition and subsequent dissipation of mechanical energy.

We started the equilibration with all atom velocities equal to zero. During the first 12.9 ps, all atoms were coupled to a heat bath [62] in order to instantly remove excess heat from the system. During all other times, heat was only exchanged through the stochastic boundary. The global coupling to a heat bath successfully reduced the temperature to 300 K within 0.2 ps and led to a very small fluctuation level of the temperature during the first 12.9 ps. The effect of the coupling to a heat bath through the stochastic boundary at times $t > 12.9$ ps can be seen as the temperature repeatedly decreases from high values caused by rescaling of the atom reference positions (see below). The coupling time of this heat exchange through the boundary can be estimated from Fig. 4 to be of the order of 20 ps and reflects the time required for conducting heat from the inside of the system to the surface.

Similar to the temperature, the energies show sharp peaks caused by the repeated rescaling of the reference positions of boundary atoms. The very fast relaxation of these energy peaks, within about 1 ps, results from the identity of the location where mechanical energy is added to the system and where heat is extracted from it, namely the boundary. Superimposed on the discontinuities and fast relaxations related with the rescaling events, the Coulomb energy and consequently the total energy undergo a slow relaxation with a characteristic relaxation time of about 50 ps. In contrast, the van der Waals energy does not show a similar slow relaxation. The relaxation of Coulombic and total energy reflects a structural change of the lipids, especially the lipid headgroups, and the adjustment of the watercaps. Fig. 4 shows that the bilayer-water system has reached equilibrium at the end of the simulation.

Pressure

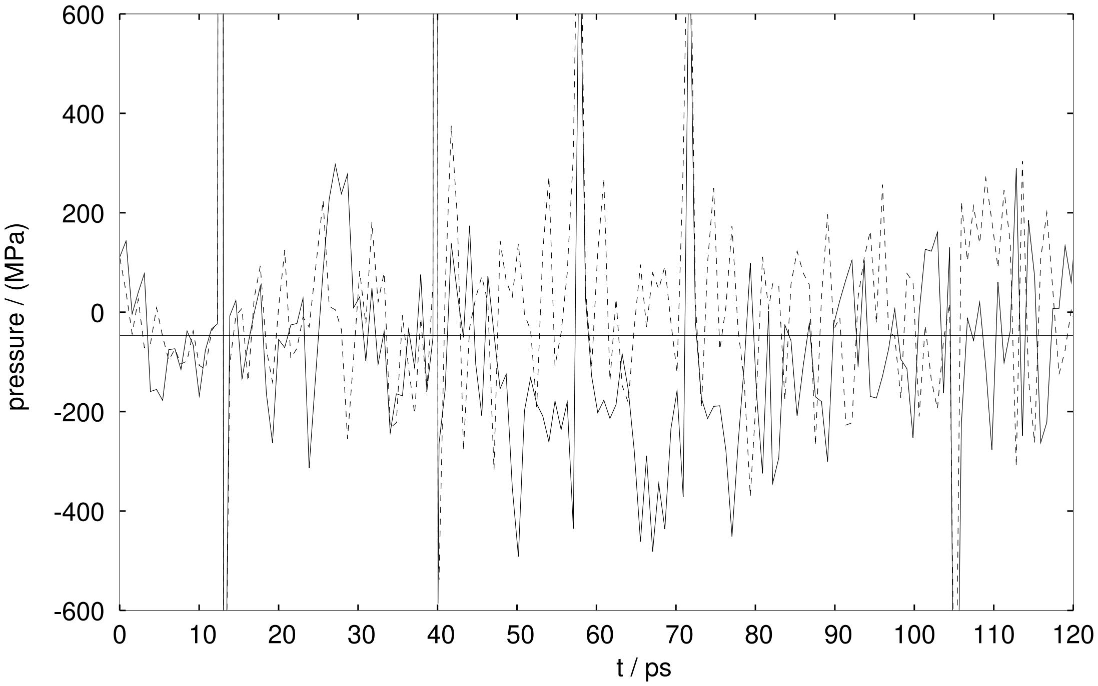

Figure 5: Pressure on the two watercap boundaries during the equilibration simulation: —, pressure on the upper ($y > 0$), and - - - , pressure on the lower ($y < 0$) boundary. The pressure was determined using the boundary method, eq 3. The horizontal line (—) marks the mean value of -46.7 ± 12.8 MPa. As with the energies, peaks in the pressure curve beyond the fluctuation level resulted from rescaling of the reference positions of boundary atoms.

While running the simulation, we found that the pressure on the boundary surfaces (see Methods) was predominantly negative, i.e., the average positions of boundary atoms were shifted towards the inside of the system when compared to the reference positions. Because the pressure, especially on the two watercaps, averaged over a time interval of 20 ps was at times deviating from -39 MPa, the estimate made for the pressure due to surface tension (see Methods), we changed the volume of the system several times by rescaling of the reference positions of boundary atoms. The rescaling factors, rescaling axes, and rescaling times were: $(0.98, xyz, 12.9\,\mathrm{ps})$, $(0.98, y, 24.6\,\mathrm{ps})$, $(0.98, y, 39.8\,\mathrm{ps})$, $(0.99, y, 57.7\,\mathrm{ps})$, $(0.99, y, 71.6\,\mathrm{ps})$ and $(1.02, y, 105.1\,\mathrm{ps})$. Except for the first rescaling event, where all three coordinates were rescaled, only the y-coordinates of the reference atoms and, therefore, only the thickness of the bilayer were affected. Each rescaling step led to a sharp increase or decrease of the boundary pressure which was very short lived, with the pressure returning to the normal fluctuation level within less than 1 ps (see Fig. 5). After some of the rescaling events, e.g., the rescaling at $t = 12.9$ ps, we observed an overshooting of the boundary pressure value in a direction opposite to the direction of the initial peak. Rescaling of the reference positions, therefore, induces a damped oscillation in the boundary.

Despite the repeated changes of the atom reference positions and the structural changes of the lipids accompanying equilibration, the pressure averaged over a 20 ps interval showed very little change when compared to the fluctuation level of the boundary pressure values. We also calculated the average of the watercap boundary pressure over the whole equlibration and found that its value, -47 MPa, is in good agreement with the value estimated to result from surface tension alone, -39 MPa. Note that the large negative pressure on the two watercaps is present mainly because of the curvature of their vacuum boundary in the equilibration setup (see Fig. 3). Other MD simulations of membrane systems report pressures of the order of -1 MPa [16] and $+25$ MPa [21], i.e., values that are also in the MPa range. We conclude that the pressure in the bilayer-water system, within a margin of about 10% of the volume enclosed by the stochastic boundary, is essentially constant and that the packing of the system during equilibration corresponds to a low internal pressure. One reason for this may be the relative "soft" nature of the harmonic restraining potential which allows the boundary atoms to adjust their positions depending on the pressure, as opposed to the situation of a periodic boundary simulation where the periodic cell dimensions have a more dramatic effect on the pressure in the system.

Simulation I

After the equilibration, we switched to a new set of partial charges which we took from the parameter and topology file `Charmm22` of CHARMm provided to us by A. MacKerell of the Department of Chemistry at Harvard [53]. We started the simulation with the structure, atom velocities and atom reference coordinates of the end of the equilibration. The reference coordinates were left unchanged during Simulation I.

Energies

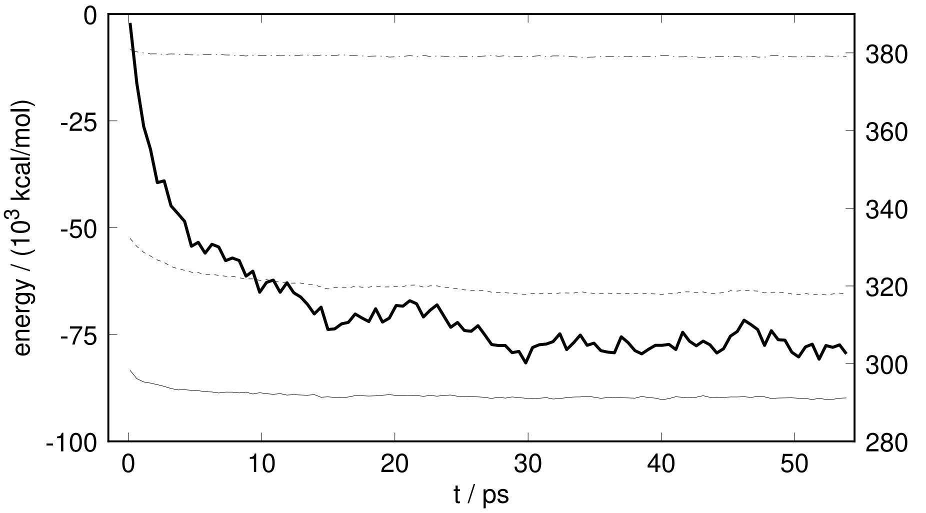

Figure 6: Energies and temperature during Simulation I: total energy (- - -), Coulomb energy (—), van der Waals energy (– · – · –), and temperature (▬). The final 25 ps of the simulation were used for analysis.

The change of the charge parameter set caused the system to be off equilibrium at the beginning of the simulation, with especially the temperature reaching a maximum of 388 K within the first picosecond. As can be seen from Fig. 6, return to equilibrium required about 30 ps. During the final 25 ps of Simulation I, which were used for analysis, the non-bonded energies as well as the temperature exhibit only minor fluctuations around their mean values, indicating that equilibrium has been reached.

Pressure

The pressure on the two watercaps (see Fig. 7), was evaluated according to the boundary method, eq 3. The pressure shows strong fluctuations around a mean value of -55.7 ± 3 MPa. This value is slightly lower than the pressure during the equilibration, which was -46.7 MPa. One reason for the decrease of the pressure may have been an improved interaction between lipid headgroups and water due to the change of the lipid partial charge set at the beginning of Simulation I. An inspection of the pressure curves in Fig. 7 suggests that the two watercap pressures are anti-correlated, even though the correlation coefficient of the two pressures is only -0.3. The anticorrelation implies that the whole assembly performs an oscillation within the potential of the harmonic restraints on the boundary.

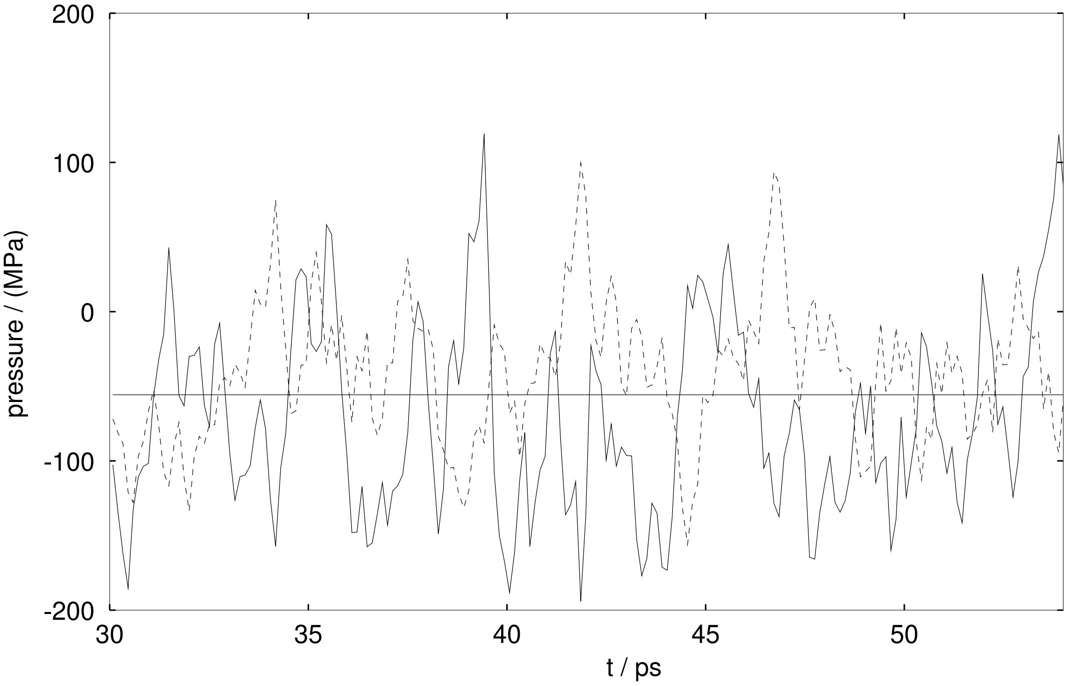

Figure 7: Pressure on the two watercap boundaries during Simulation I: —, pressure on the upper ($y > 0$), and - - -, pressure on the lower ($y < 0$) boundary. The pressure was determined using the boundary method, eq 3. The horizontal line (—) marks the mean value of -55.7 ± 3 MPa.

Diffusion

In order to calculate the diffusion coefficients of POPC, we determined the average displacement of the center of mass of the lipids. The average displacement curves in Fig. 8 exhibit two different time domains: a short-time domain from 0 ps to 2 ps and a long-time domain from 4 ps to 25 ps with different diffusion behavior. From a linear regression fit to the $\langle \xi^2 \rangle$-curves in Fig. 8, we determined according to eq 12 $D^{\ell}_{\text{lat}} = 0.023 \cdot 10^{-5}\,\text{cm}^2/\text{s}$ as the lateral and $D^{\ell}_{\text{tra}} = 0.115 \cdot 10^{-5}\,\text{cm}^2/\text{s}$ as the transversal long-time diffusion constants. In a similar way, we determined the short-time diffusion constants for the time range up to 2 ps as $D^{\text{s}}_{\text{lat}} = 0.296 \cdot 10^{-5}\,\text{cm}^2/\text{s}$ and $D^{\text{s}}_{\text{tra}} = 0.499 \cdot 10^{-5}\,\text{cm}^2/\text{s}$. These values of the diffusion constants are of the same order of magnitude as experimental findings for a DPPC membrane containing 12 wt% of water (the backscattering spectroscopy used in the experiment covers motions with relaxation times of $10^{-8} \dots 10^{-10}$ s, which is barely in the range of our simulations) reported in [5]: $D^{\ell}_{\text{lat}} = 0.0097 \cdot 10^{-5}\,\text{cm}^2/\text{s}$ and $D^{\text{s}}_{\text{lat}} = 0.015 \dots 0.6 \cdot 10^{-5}\,\text{cm}^2/\text{s}$ and $D^{\text{s}}_{\text{tra}} = 0.21 \cdot 10^{-5}\,\text{cm}^2/\text{s}$. However, König et. al. note that these diffusion coefficients "should

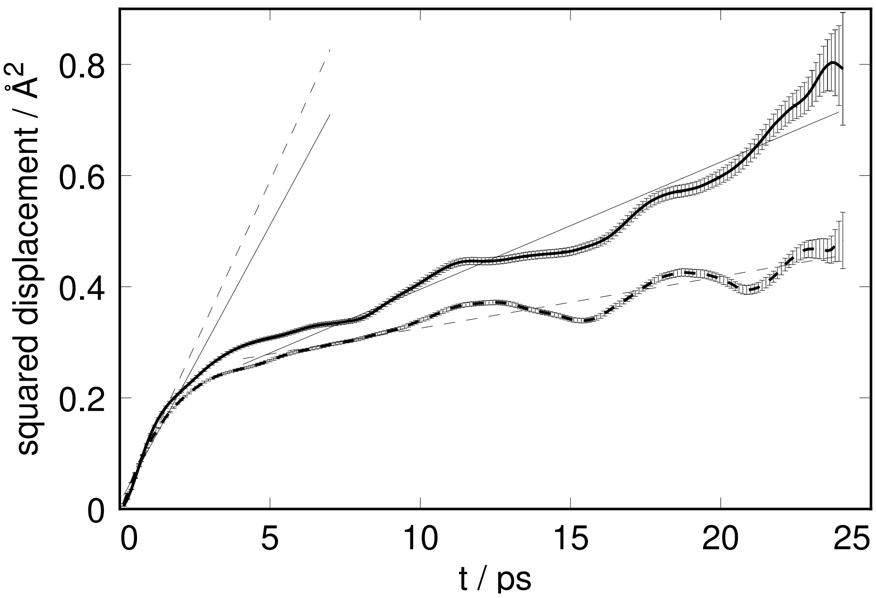

Figure 8: The transversal (—, upper curve) and lateral (- - -, lower curve) average square displacement $\langle \xi^2 \rangle$ of the center of mass of a lipid molecule in the bilayer water system during Simulation I. The error bars show the standard deviation of the displacement values (see eq 14). The straight lines result from a linear regression fit to the $\langle \xi^2 \rangle$-curves in two different time domains (see text).

be handled with care" as the underlying model assumptions[6] are an oversimplification and furthermore their measurements were done on a DPPC sample in the liquid-crystalline phase [63].

Area per Head Group

Using the procedure described in Methods, we determined the average area per POPC head group at the end of Simulation I as $A = 46.3 \pm 0.01\,\text{Å}^2$. Nagle and Wiener [38] determined experimental values of the average area per DPPC headgroup in three different membrane phases: for the crystal phase (L_c) at 0^o C $A = 45.8\,\text{Å}^2$, for the gel phase ($L_{\beta'}$) at 20^o C $A = 48.5\,\text{Å}^2$, and for the fluid phase (L_α) at 50^o C $A = 57.6\ldots70.9\,\text{Å}^2$. Wiener and White [51] give experimental values for DOPC of $A = 40\,\text{Å}^2$ in the crystalline all-trans phase and $A = 60\,\text{Å}^2$ in the liquid-crystal phase (L_α). Since POPC differs from DPPC through the addition and from DOPC through the deletion of one double bond segment (–CH=CH–), one can expect that the average area per headgroup of POPC is in between those for DPPC and DOPC. A comparison, therefore, suggests that the bilayer during Simulation I which was done at $T = 27^o$ C is in the crystal or gel phase.

[6]König et. al. assume in their model that the proton motions in the fatty acid tail of a lipid are completely independent of each other, which is of course not valid for protons within one molecule.

Order Parameters

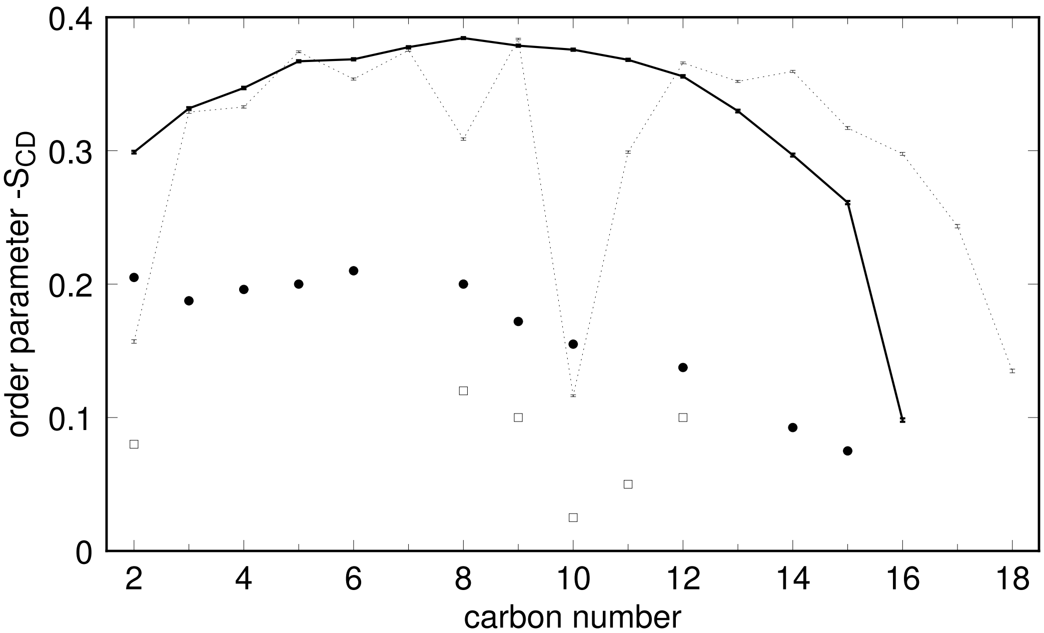

Figure 9: Deuterium order parameter profile of the sn-1 (—) and sn-2 chain (- - -) of POPC as determined from Simulation I. For comparison, the experimental results of [64] for the palmitoyl chain (●) and for the oleic chain (□) [65] of POPC in the fluid phase at 27^o C are also given. The abscissa refers to a numbering scheme where the fatty acid carbons are numbered consecutively, starting with 1 at the ester carbon. Error bars indicating the standard deviation of the simulation values are too small to be represented. The connecting lines serve as a visual guide.

We determined the order parameter profile of both fatty acid tails of POPC (see Fig. 9). For the unsaturated oleoyl tail, we found a pronounced odd–even alteration of the order parameter as a function of carbon number which is not present in the profile of the saturated palmitoyl chain. Both profiles show a plateau which is also observed in experiments [66, 64, 37], even though the decrease of the experimental order parameter $-S_{\rm CD}$ towards the end of the palmitoyl chain begins at a lower carbon number than in the calculated profile. The absolute value of the calculated order parameters in Fig. 9 is about two times larger than the absolute value of the experimental order parameters which were determined from POPC in the fluid phase. For carbon number 2 the absolute value of the simulated order parameters are lower than those for carbon number 3, while the opposite is true for the experimental values. The comparison of the calculated with experimental order parameter profiles indicates that during Simulation I, the simulated bilayer was not in the liquid crystal phase but rather in the gel phase, where the molecular order is higher. Unfortunately, no experimental data on the gel phase are available for comparison.

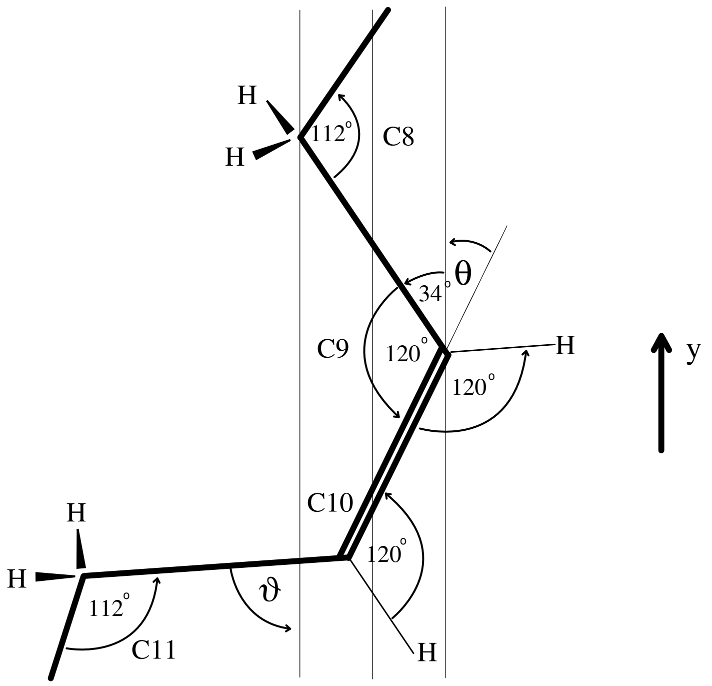

Figure 10: Sketch of the idealized geometry of the vicinity of the *cis*-double bond. It is assumed that the segments from C2 to C8 are perfectly aligned with the bilayer normal (vertical lines). Angles of 112^o and 120^o have been assumed for sp^3 and sp^2 hybridization of carbon atoms, respectively [60].

Both the experimental data and our simulation data show a characteristic dip in the order parameter profile for the second double bonded carbon atom (C9). As pointed out by [60] two factors contribute to the order parameter (see eq 10): (i) the orientation of the C–H bond vector, expressed through the angle θ with the bilayer normal (see Fig. 10), and (ii) the orientational fluctuations of the C–H bond vector. The method of MD simulations allows measurement of each factor independently, and therefore establishes which contribution dominates.

The average angle of the double bond with the bilayer normal was measured for the upper layer at $\theta_u = 23.22 \pm 0.14^o$ and for the lower layer at $\theta_l = 22.17 \pm 0.13^o$. These values are less than what one would expect ($\theta = 26^o$) for a perfect (except for the *cis*-double bond) all-*trans* chain with the segment from C2 to C8 perfectly aligned with the bilayer normal (see Fig. 10). The high values of the order parameter $-S_{\rm CD} \approx 0.4$, close to the highest value of $-S_{\rm CD} = 0.5$, indicate that these segments are indeed highly ordered and well aligned with the bilayer normal. The average angle of the bond segment C10–C11 was determined for the upper layer at $\vartheta_u = 57.05 \pm 0.20^o$ and for the lower layer at $\vartheta_l = 62.41 \pm 0.19^o$.

Again these values are lower than what one would expect for a perfect geometry ($\vartheta = 86^o$). This deviation is a result of the tight packing in the gel phase which tends to realign the hydrocarbon segments C11 to C18 with the bilayer normal and hence changes the angles in the observed fashion.

The local chain order parameter is $\mathbf{S}_{zz} = 0.7541 \pm 0.0013$ for the C=C bond and $\mathbf{S}_{zz} = -0.0478 \pm 0.0018$ for the following C10–C11 segment. This is in good agreement with values computed only from the average angles θ and ϑ given above, namely for the C=C bond $\mathbf{S}_{zz}(\theta) = 0.76 \ldots 0.79$ and for the following C10–C11 segment $\mathbf{S}_{zz}(\vartheta) = -0.05 \ldots -0.18$. This confirms the conclusion of [60] that the dip in the order parameter profile is not due to increased fluctuations but that it is rather a pure geometric effect.

Distribution of Molecular Groups

A recent publication by Wiener and White [51] provides detailed structural information about fluid DOPC bilayers that can readily be used for comparison with our simulation. We use a similar parsing scheme as described by Wiener and White (see Fig. 1). One obvious difference is that we have a palmitoyl chain instead of an oleoyl chain at the sn-1 position. When comparing the calculated density profiles of lipid segments (see Fig. 11) with

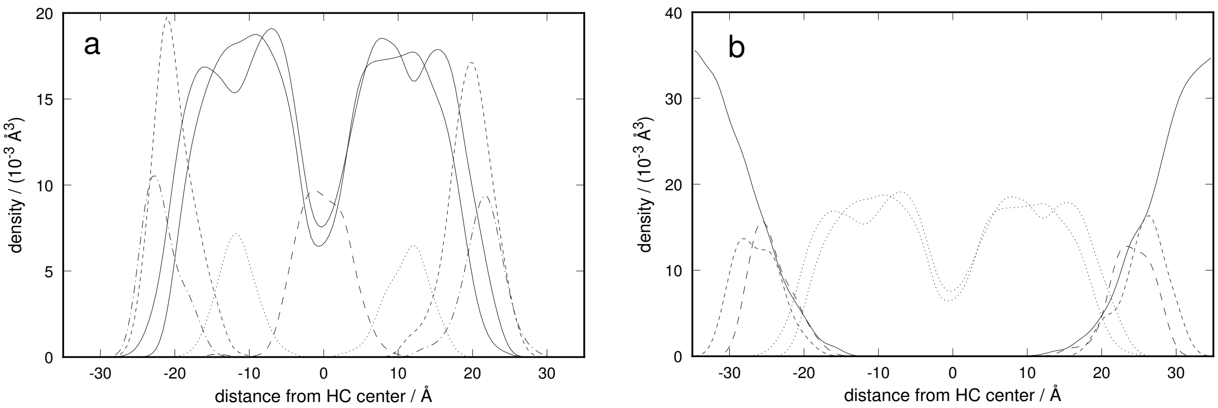

Figure 11: Cross-membrane density profiles of atom groups of the bilayer-water system as specified in Fig. 1. a) lipid tail region: methylene groups (CH_2, —) of the sn-1 and sn-2 chain, methyl groups (CH_3, – – –), ester groups (- - -), double bonded carbons (....), and glycerol backbone (–·–·–·); b) head group and water region: water (—), choline (- - -), and phosphate (– – –). The methylene groups (.....) are shown as a reference. The profiles were calculated by averaging static profiles (see Methods) over the last 25 ps of Simulation I.

the experimental profiles shown in Figs. 18 b and 19 b, it becomes evident that the bilayer is much thicker in Simulation I than in the liquid-crystal phase that was measured in the experiment. The pronounced dip in the CH_2 distribution at the center of the bilayer in Fig. 11 a shows that there is little overlap of the tails of the two monolayers. The two dips in the CH_2 distribution of the sn-2 chain at ±12 Å coincide with the peaks of the double bond distributions as both have the same origin, namely the substitution of a –CH_2–CH_2– segment by a –CH=CH– segment. The sn-2 oleoyl chain, which is two carbon segments longer than the sn-1 palmitoyl chain has not only a higher density of CH_2 groups than the palmitoyl chain at the center of the bilayer ($7.7 \cdot 10^{-3}\text{Å}^3$ compared to $6.4 \cdot 10^{-3}\text{Å}^3$), but it also extends about 1.76 Å further towards the head group region.

Two Disasters

The analysis of Simulation I led to the conclusion that the simulated bilayer is in the gel phase rather than the liquid-crystal phase, which is the biologically most relevant phase [36]. Perhaps the most important difference between the bilayer of Simulation I and experimental data on liquid-crystal phase bilayers is the area per lipid molecule, which is too small by a factor of 1.5. We, therefore, decided to increase the area per lipid molecule from 46.3 Å^2, the value during Simulation I, to the experimental value known for the liquid-crystal phase, namely 70 Å^2 [10, 51], and eventually induce a phase change in the system as an effect of the surface area increase. In the following, we report on two attempts at inducing this change which we deemed unsuccessful.

"Disaster I": Separation of the Monolayers

In our first attempt to increase the area per lipid molecule by a factor of 1.5, we rescaled the x and z-coordinates of the reference positions that were used during Simulation I by a factor of 1.23 while leaving the y-coordinates unchanged. We thereby increased both the lateral area and the volume of the system by a factor of 1.5, intending to readjust the bilayer thickness and internal pressure at a later time.

We started the simulation using the final structure and atom velocities of Simulation I and using the rescaled reference positions to calculate the restraining forces on atoms. During the simulation, we monitored energies and boundary pressure in the system. Initially, the restraining energy was increased by 11,300 kcal/mol when compared to the energy at the end of Simulation I. As a consequence of this relatively small perturbation (compare "Disaster II") the temperature raised to a moderate maximum value of 340 K after 0.1 ps of simulation time. The two non-bonded energies showed qualitatively different behavior: While the Coulomb energy decreased throughout the simulation, the van der Waals energy increased during the first 3 ps by 3,000 kcal/mol and then decreased by 600 kcal/mol until the end of the simulation. During "Disaster I", therefore, the system never regained the van der Waals energy lost during the initial phase of structural reorganization which indicates a disruption of good contacts in the lipid tail region.

After the system had reached equilibrium, we displayed the structure on a graphics terminal and found that, except for the lipids in the boundary which were restrained, the two monolayers had separated (see Fig. 12). From this, it became clear that a volume increase by 50% was, even for a short time interval of the order of 10 ps, beyond the limit of what the system could adjust to while preserving the integrity of the bilayer. Despite the ability of the stochastic boundary to compensate volume changes in a 10% range (see Equilibration), the low internal pressure in the system led to the creation of a hole at the location of weakest

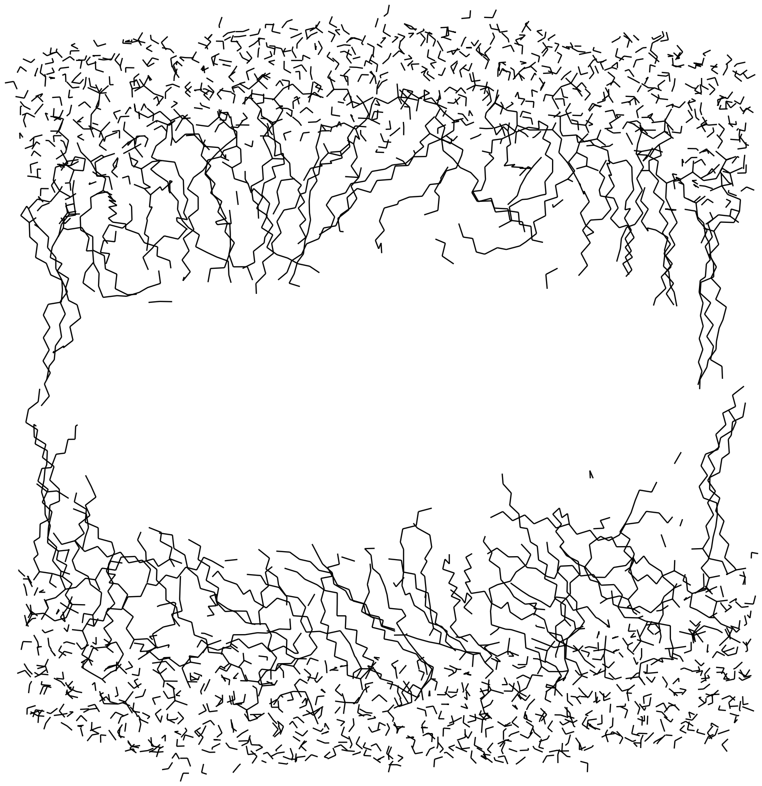

Figure 12: Line drawing of molecules within a 20 Å slice through the membrane water system at the end of the "Disaster I" simulation. The slice is parallel to the xy-plane. Only atoms for which the z-coordinates satisfy $|z| < 10$ Å are shown, such that some of the molecules appear incomplete.

interaction between molecules, namely the area of van der Waals contact between the monolayers. We concluded that all further changes in the setup of the system should meet the requirement of volume conservation.

"Disaster II": Thermal Disintegration

In our second attempt to increase the average area per POPC headgroup, we rescaled the x and z-coordinates of the atom reference positions by a factor 1.23 and the y-coordinates of the reference positions by 0.66 before starting the simulation, thus keeping the volume of the system constant. We also changed the restraining force constants on lipid atoms. Only the phosphorus atoms of the lipids were subject to a restraining potential, with the maximum force constant $k_{\max}$ reduced by a factor 5 (see Methods). We otherwise proceeded in exactly the same way as described in "Disaster I", above. Especially, the restraining potential with respect to the watercaps was not changed.

After starting the simulation, we observed an initial 1 ps phase of interconversion of the restraint energy into other potential energies and heat, followed by a relaxation phase during which energies and temperature decreased rapidly. This time, the restraint energy at the

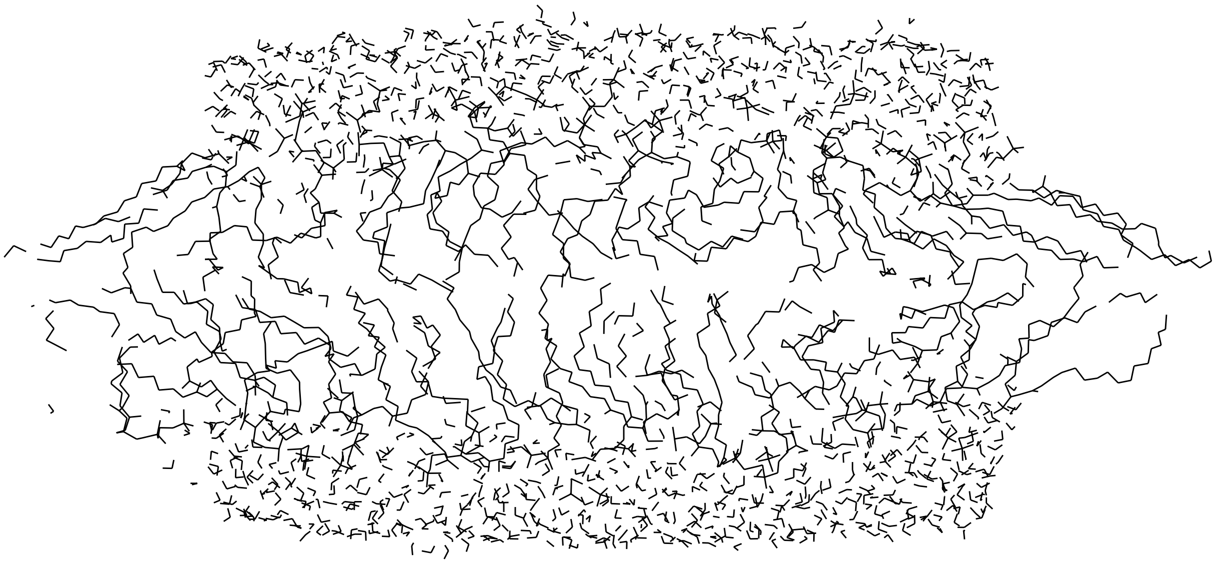

Figure 13: Line drawing of molecules within a 20 Å slice through the membrane water system at the end of the "Disaster II" simulation. The slice shown is parallel to the xy-plane. Only atoms for which the z-coordinates satisfy $|z| < 10$ Å are shown, such that some of the molecules appear incomplete.

beginning of the simulation was as much as $4 \cdot 10^5$ kcal/mol higher than the restraint energy at the end of Simulation I, and the maximum temperature reached was 1,020 K, compared to a maximum temperature of 340 K during "Disaster I".

When displaying the system after 3 ps of simulation time on a graphics screen, we observed two potentially pathological features of the structure: a large number of water molecules had escaped through the stochastic boundary, and, more importantly, the tails of lipid molecules in the lateral boundary region were pointing outwards into the vacuum in a manner that looked very much like the result of an explosion (see Fig. 13). Both the high temperature reached during the simulation and the distortion of the stochastic boundary after rescaling are possible reasons for the escape of unrestrained water molecules from the system. As a cause of the extreme distortion of lipid tails in the lateral boundary, we considered the change from restraining all lipid atoms in the boundary to restraining phosphorus atoms only. This idea, however, could be ruled out after analyzing Simulation II (see below) in which the same restaining potential was used but no similar effect on the boundary lipids was observed. The extreme disorder of the boundary lipid tails was, therefore, also a consequence of the high temperature reached during the "Disaster II" simulation, which in turn was caused by the high restraint energy at the beginning of the simulation. We did not continue the simulation beyond the 3 ps reported here even though the bilayer may have eventually reached a new equilibrium. Instead, we decided to proceed in a more cautious way when changing the system setup and to avoid restraint energy increases of the order of 15 kcal/mol per atom in the system which had proven to drive the system far from equilibrium.

Simulation II

To avoid high restraint energies in setting up Simulation II, we performed a molecular rescaling (see Methods) of the x and z-coordinates of both the reference positions and the actual atom positions as obtained at the end of Simulation I. The scaling factor used for x and z was 1.23, leading to an expected increase of the lateral area by 50%. New watercaps with a simple, rectangular geometry were added on both sides of the bilayer (see Construction of the Membrane Bilayer). We then rescaled the y-coordinates of all reference positions by a factor of 0.66 in order to guide the system to an equilibrium with volume and density equal to the values during Simulation I. The main difference between the system setup of the "Disaster II" simulation and of Simulation II is the shifting in x and z-direction of all atoms to locations near their respective reference positions, through molecular rescaling of the actual coordinates. After starting the simulation, this led to a total restraint energy in the system of $2 \cdot 10^5$ kcal/mol, which was only 50% of the restraint energy at the beginning of "Disaster II."

Energies

As had already been observed during the Disaster simulations, the system needed time to adjust to the new setup. The non-bonded energies and the temperature decreased continuously during the first 10 ps of the simulation (see Fig. 14), which is considered an equilibration phase. During the time from 10 ps to 56 ps of Simulation II, which is used in the subsequent analysis, the energies and temperature show only typical equilibrium fluctuations.

Pressure

The values of the pressure on the top and bottom surface at the beginning of Simulation II were very high ($\approx 7,500$ MPa) because in this direction only the reference positions were rescaled. The pressures on the other surfaces deviate only slightly from their respective means, because in those directions the actual atom positions were also rescaled by molecular rescaling (see Methods). In the x and z-directions, the average values of the pressure are $\overline{p(x)} = -19.7 \pm 0.54$ MPa and $\overline{p(z)} = -18.8 \pm 0.42$ MPa respectively, which is approximately 16 MPa higher than the estimated contribution from the surface tension $p_{\mathrm{surf}} \approx -36$ MPa. The average value of the pressure in y direction is $\overline{p(y)} = -9.6 \pm 0.53$ MPa. This is about 46 MPa less than the average value in Simulation I (−56 MPa), as here the contribution of the surface tension (40 MPa) is missing because the watercaps in Simulation II are flat. The fluctuations of the pressure on the six boundary surfaces, as depicted in Fig. 15, are much smaller than those during the Equilibration (see Fig. 5) and Simulation I (see Fig. 7). We determined the correlation coefficients of the pressures on opposing surfaces and found a significant anticorrelation. For example, in the case of the two watercap boundaries the correlation coefficient was −0.72. The anticorrelation of pressures on opposing surfaces suggests that the whole system performs oscillations in the potential of the harmonic restraints.

Diffusion

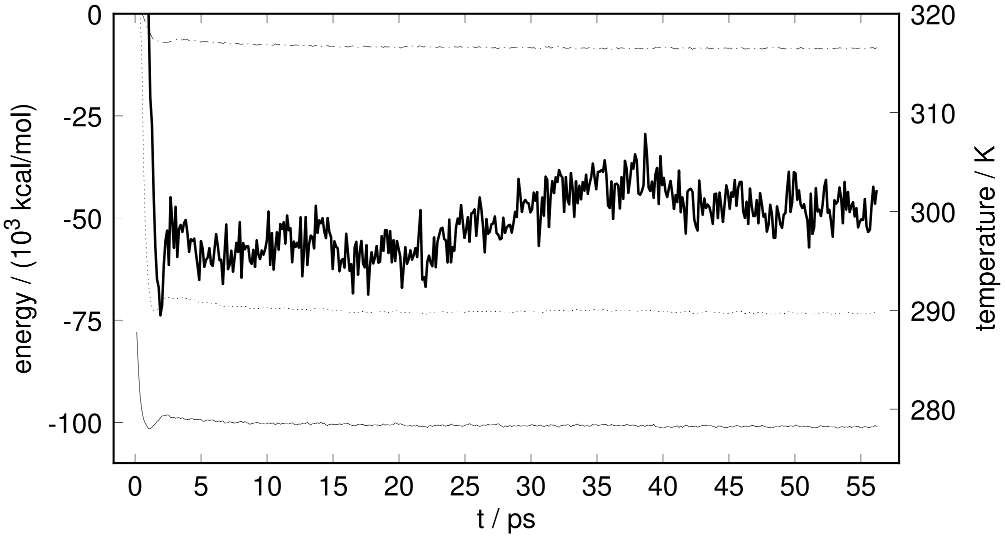

Figure 14: Energies and temperature during Simulation II: total energy (- - -), Coulomb energy (—), van der Waals energy (– · – · –·), and temperature (▬). During the first ps, the energies and temperature reached maximum values of $E_{\text{tot}} = 211.3 \cdot 10^3$ kcal/mol, $E_{\text{vdW}} = 0.53 \cdot 10^3$ kcal/mol, $E_{\text{Coul}} = -77.8 \cdot 10^3$ kcal/mol and $T = 767.8$ K (some peaks outside plot range), as a result of the high potential energy of the setup after the induction of the phase transition. The final 46 ps of the simulation were used for analysis.

The average displacement curves in Fig. 16 exhibit two different time domains, similar to those observed in Simulation I: a short-time domain from 0 ps. . . 2 ps and a long-time domain from 4 ps . . . 46 ps. From a linear regression fit to the $\langle \xi^2 \rangle$-curves in Fig. 16, we calculated (eq 12) $D^{\ell}_{\text{lat}} = 0.073 \cdot 10^{-5}\,\text{cm}^2/\text{s}$ as the lateral and $D^{\ell}_{\text{tra}} = 0.102 \cdot 10^{-5}\,\text{cm}^2/\text{s}$ as the transversal long-time diffusion constants. Similarly the short-time diffusion constants for the time range up to 2 ps have been determined as $D^{\text{s}}_{\text{lat}} = 0.324 \cdot 10^{-5}\,\text{cm}^2/\text{s}$ and $D^{\text{s}}_{\text{tra}} = 0.465 \cdot 10^{-5}\,\text{cm}^2/\text{s}$.

The long-time lateral diffusion constant D^{ℓ}_{lat} has increased by a factor of 3 compared to its value in Simulation I, while the other diffusion constants are of comparable size. Increasing the area per head group provided more room for the lipids to diffuse laterally, while it had only minimal influence on the transversal diffusion. The short-time diffusion is also not influenced by this change.

It is not to be expected that lipids would exchange places ("hopping") on a timescale as short as the one covered by this simulation, as can be seen by estimating the time one lipid needs to explore the area per head group $A = 65.5\,\text{Å}^2$ (see following section): $\tau = A/D^{\ell}_{\text{lat}} \approx$ 10 ns. This estimate also agrees well with the typical jump frequencies for lipids, which are in the order of $\nu \approx 10^7 \ldots 10^8$/s [67, 68]. If this time is divided by the number of simulated

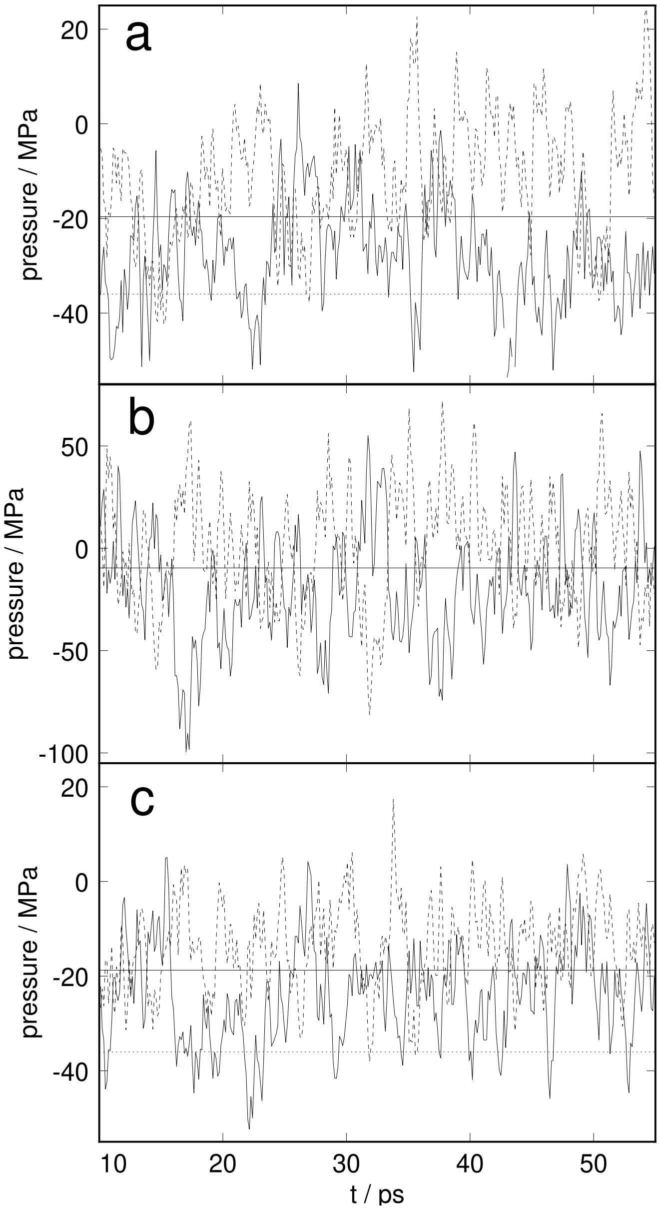

Figure 15: Pressure during Simulation II on a) the two lateral boundaries parallel to the yz-plane, b) the two watercap boundaries, and c) the two lateral boundaries parallel to the yx-plane: —, pressure on the upper $(x, y, z > 0)$, and - - -, pressure on the lower $(x, y, z < 0)$ boundary, respectively. The pressure was determined using the boundary method, eq 3. The horizontal dotted line (....) in a) and c) marks the pressure due to surface tension in a bilayer with thickness $R = 39\,\text{Å}$ (peak to peak of choline distribution in Fig. 19 a, see Methods). The horizontal continuous lines (—) indicate the average values of the pressures.

lipids $N = 200$, one obtains an estimate for the average time until one of the lipids in the patch will exchange its place with a neighbor $\tau/N \approx 45\,\text{ps}$. Therefore one would expect to

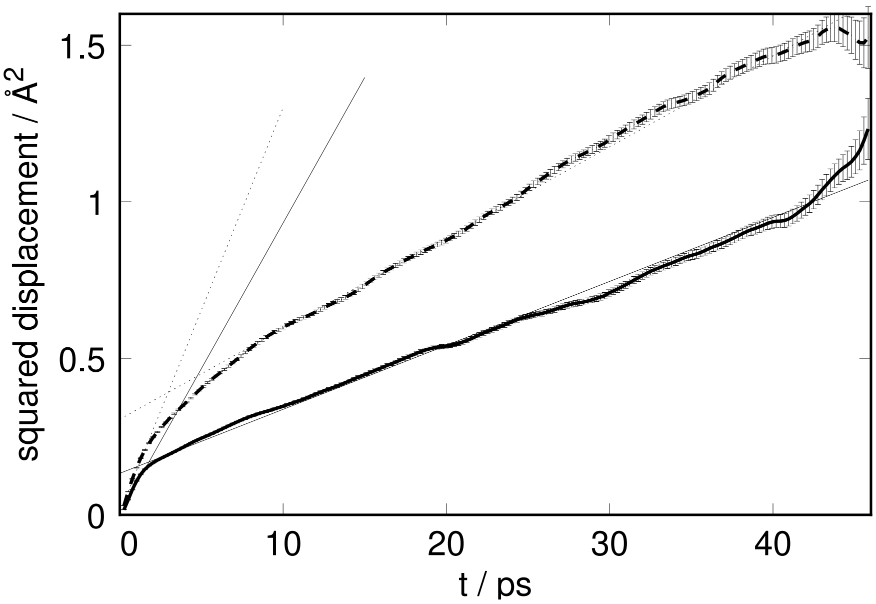

Figure 16: The transversal (— lower curve) and lateral (- - - upper curve) average square displacement $\langle\xi^2\rangle$ of the center of mass of a lipid molecule in the bilayer water system during Simulation II. The error bars show the standard deviation of the displacement values (see eq 14). The straight lines result from a linear regression fit to the $\langle\xi^2\rangle$-curves in two different time domains (see text).

see only one event over the course of the simulation, which demonstrates that D^{ℓ}_{lat} does not describe the hopping of lipids.

[67] report a value of $D^{\ell}_{\mathrm{lat}} = 0.07 \cdot 10^{-5}\,\mathrm{cm}^2/\mathrm{s}$ for pyrene in DOPC at $T = 30^o\,\mathrm{C}$ in the liquid-crystalline phase, which translates through application of the free volume model of diffusion [69] to $D^{\ell}_{\mathrm{lat}} = 0.036 \cdot 10^{-5}\,\mathrm{cm}^2/\mathrm{s}$ as the self-diffusion coefficient for DOPC. [68] report $D^{\ell}_{\mathrm{lat}} = 0.02 \cdot 10^{-5}\,\mathrm{cm}^2/\mathrm{s}$, $D^{\ell}_{\mathrm{tra}} = 0.24 \cdot 10^{-5}\,\mathrm{cm}^2/\mathrm{s}$.

Area per Head Group

The lipid density is one of the adjustable parameters of the stochastic boundary simulation method. It can be predetermined by rescaling the reference positions. According to [70], the area per lipid for DPPC in excess water is $A = 70\,\mathrm{Å}$; the rescaling of the reference positions was done such as to achieve this value. However, in the course of the simulation, the area per head group stabilized at a value of $65.5 \pm 0.04 \mathring{A}^2$. This is probably induced by the positive value of the lateral surface pressure, but a value of $A = 65\,\mathrm{Å}^2$ is still in good agreement with the experimental values for the liquid-crystal phase of membranes. Nagle and Wiener [38] give experimental values for A for DPPC in the fluid phase (L_α) at $50^o\,\mathrm{C}$ of $A = 57.6 \ldots 70.9\,\mathrm{Å}^2$. Wiener and White [71, 51] give experimental values for A for DOPC of $A = 60\,\mathrm{Å}^2$ in the liquid-crystal phase. Therefore, the density data given above warrant the conclusion that our sample (which is simulated at $T = 27^o\,\mathrm{C}$) is in the liquid-crystal phase.

Order Parameters

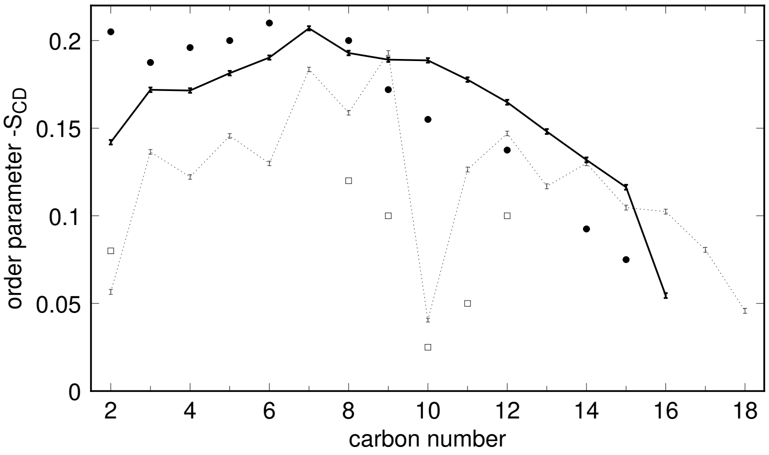

Figure 17: Deuterium order parameter profile of the sn-1 (—) and sn-2 chain (- - -) of POPC as determined from Simulation II. For comparison, the experimental results of [64] for the palmitoyl chain (•) and for the oleic chain (□) [65] of POPC in the fluid phase at 27^o C are also given. The abscissa refers to a numbering scheme where the fatty acid carbons are numbered consecutively, starting at the ester carbon with 1. Error bars indicate the standard deviation of the simulation values. The connecting lines serve as a visual guide.

The shape of the order parameter profiles obtained from our simulation according to eq. 11 (see Fig. 17) is similar to the one obtained in experiments [64]. However, the values for carbons close to the glycerol backbone are too low, while those towards the hydrocarbon end are too high. This is due to the short simulation time of only 56 ps, as profiles computed from 5 ps time intervals progressively approached the experimental values as the intervals are shifted towards the end of the simulation. Compared to the gel simulation (cf. Fig. 9), the values are now much closer to the experimantal data for the liquid-crystal phase of POPC. As already observed in the gel phase, the unsaturated oleoyl chain shows a strong odd–even alteration of the order parameter with carbon number, while the order parameters of the saturated palmitoyl chain do not exhibit this behavior. The typical increase in the order parameter for carbon atom number 2 found in many experiments [72, 73, 64, 74] is not reproduced by these simulations. Results similar to ours were previously obtained in other simulations [23, 22].

The average angle of the double bond with the bilayer normal was measured for the upper layer at $\theta_u = 37.96 \pm 0.19^o$ and for the lower layer at $\theta_l = 38.89 \pm 0.20^o$. This value is larger than what would be expected ($\theta = 26^o$) for a perfect (except for the *cis*-double bond) all-*trans* chain with the segment from C2 to C8 perfectly aligned with the bilayer normal (see also Fig. 10). The low values of the order parameter $-S_{\rm CD} \approx 0.17$ indicate that the last assumption is not true for liquid-crystal bilayers. The increased area per head group, compared to Simulation I, allows for more motional freedom of the hydrocarbon tails. This explains the larger value of $\theta \approx 38^o$ compared to the value of 22.5^o in Simulation I. However, this value of $\theta \approx 38^o$ does not agree with the value of $\theta = \pm 9^o$ reported by [60] for liquid-crystal POPC bilayers at $T = 27^o$ C.

The average angle of the bond segment C10–C11 with the bilayer normal was measured for the upper layer at $\vartheta_u = 67.97 \pm 0.25^o$ and for the lower layer at $\vartheta_l = 63.12 \pm 0.23^o$. These values are lower than what would be expected for a perfect geometry ($\vartheta = 86^o$); however, they are higher than the value obtained in Simulation I ($\vartheta = 60^o$). The deviation from the ideal-geometry value is due to the tight packing which tends to realign the hydrocarbon segments C11 to C18 with the bilayer normal, while the increase of θ and ϑ compared to Simulation I is caused by the increase in lateral area per lipid, which relaxes the very tight packing found in the gel phase.

The local chain order parameter is $\mathbf{S}_{zz} = 0.395 \pm 0.002$ for the C=C bond and $\mathbf{S}_{zz} = -0.063 \pm 0.002$ for the following C10–C11 segment. This is in good agreement with values computed only from the average angles θ and ϑ given above, namely for the C=C bond one finds $\mathbf{S}_{zz}(\theta) = 0.41 \ldots 0.43$ and for the following C10–C11 segment $\mathbf{S}_{zz}(\vartheta) = -0.19 \ldots -0.29$. This is in good agreement with the experimental value of $\mathbf{S}_{zz} = 0.37 \pm 0.04$ reported by [60] for the C=C bond. Our simulation supports the conclusion of [60] that the dip in the order parameter profile is not due to increased fluctuations but that it is a geometric effect. However, the main conclusion of [60], namely that the segmental fluctuations in POPC bilayers are not dependent on the segment geometry but are only determined by the distance of the segment from the lipid-water boundary, cannot be supported by our simulations, as is outlined below in Section "Thermal Motion." Instead, it can be stated that the increased fluctuations of the double bonded carbons are overshadowed in the order parameter profile by an effect caused by the different geometry of the *cis*-double bond. Furthermore, only one double bonded carbon atom (C10) shows the strong dip in the order parameter profile, while both double bonded carbon atoms (C9, C10) have increased RMS values (see Fig. 24). This also suggestes that the dip in the order parameter profile for the double bonded carbon atom (C10) and the increased RMS values of both double bonded carbons are independent of each other.

Distribution of Molecular Groups

The distribution of molecular groups in our simulation (see Figs. 18 a, 19 a) agrees well with the experimental results on DOPC of [51] (see Figs. 18 b, 19 b). The maximum values, representing the average positions of the quasimolecular fragments, are slightly closer to the center of the bilayer in our simulation than in the experiment. In our simulation the phosphate group on the average is located at 17.8 Å and −17.5 Å for the upper and lower layer respectively, while [51] locate this group at 20.15 Å. The same applies to the choline group which can be found in our simulation at 19.3 Å and −19.1 Å for the upper and lower layer respectively, while [51] find a value of 21.86 Å. The pronounced dip in the CH_2 distribution

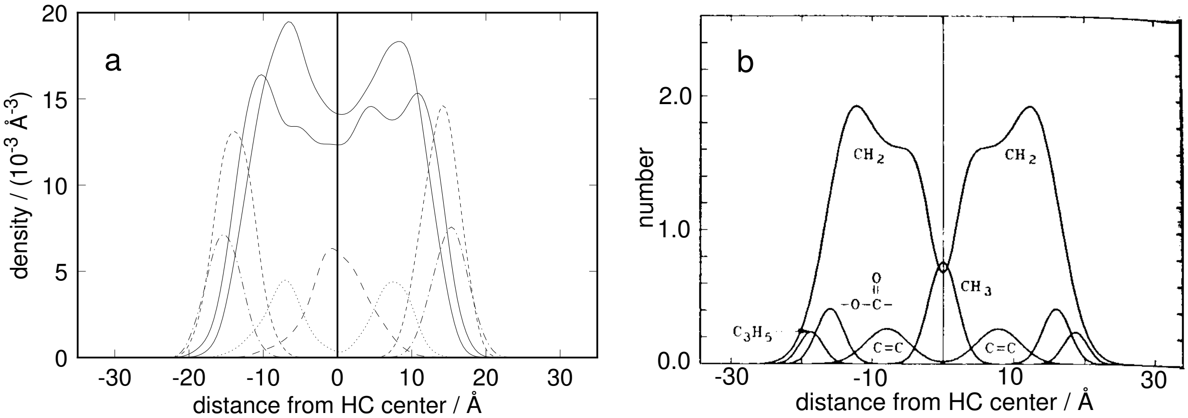

Figure 18: Cross-membrane density profiles of atom groups within the lipid tails as specified in Fig. 1: methylene groups (CH_2, —) of the sn-1 and sn-2 chain, methyl groups (CH_3, – – –), ester groups (- - -), double bonded carbons (....), and glycerol backbone (–·–·–·). The distance is measured relative to the center of the hydrocarbon (HC) area. a) profiles averaged over the last 46 ps of Simulation II; b) for comparison, experimental results for DOPC in number density units (figure adapted from [51]).

at the center of the bilayer which was present in Simulation I (see Fig. 11 a) has disappeared in Simulation II indicating a much stronger interdigitation of the two bilayers in the liquid-crystal phase compared to the gel phase. Compared to Simulation I the distribution of the double bonds has shifted towards the center of the bilayer. In agreement with the experimental data (see Fig. 18 b) there is a non-zero probablility to find C=C segments at the bilayer center.

A major difference between Fig. 18 a and Fig. 18 b lies in the distribution of the methylene groups relative to the head group. While Wiener & White see a substantial number of CH_2 groups extending beyond the glycerol backbone towards the solvent, in our simulation the CH_2 groups are not found beyond the backbone region.

A comparison of Fig. 19 a and b shows that there is less water penetration into the head group region (choline and phosphate groups) in our simulation than suggested by the experimental data. This can be attributed to the short simulation time of 240 ps (this number includes the times of the Equilibration, Simulation I, and Simulation II). The declining water density for distances of more than 32 Å from the center in Fig. 19 a marks the boarder of our simulation area, while the decrease in water density in Fig. 19 b marks the onset of the next membrane in a stack of multilamellar membranes.

Analysis of Head Group Region

We have determined the head group orientation as expressed by the average angle $\alpha = \angle(\overline{\mathrm{P\,N}}, y)$. For the upper layer we obtain $\alpha = 69.44 \pm 0.26^o$ and for the lower layer $\alpha = 112.46 \pm 0.24^o$. This translates into an azimuth of the head group above the bilayer plane of 20.56^o and 22.46^o, for the upper and lower layer respectively, and is in excellent agreement

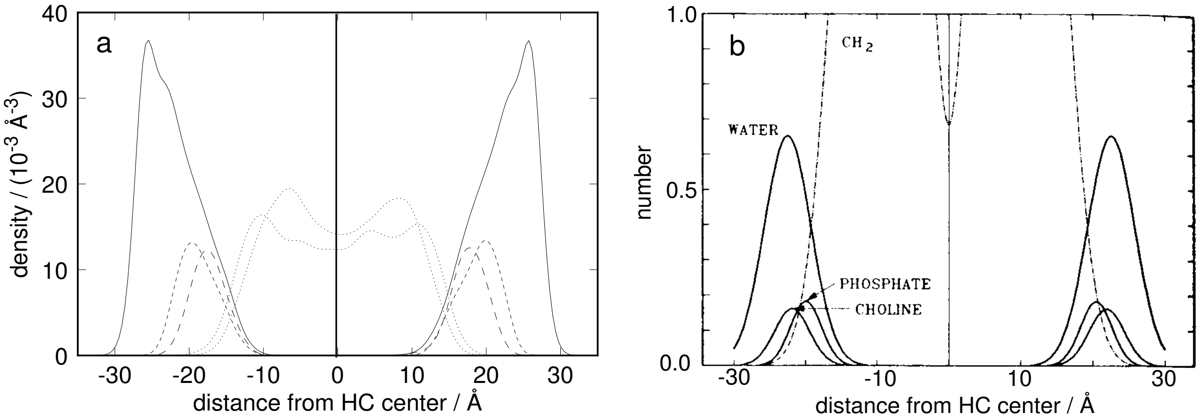

Figure 19: Cross-membrane density profiles of atom groups within the lipid head group region and of water as specified in Fig. 1: water (—), choline (- - -), and phosphate group (– – –). The methylene groups (....) are shown as a reference. The distance is measured relative to the center of the hydrocarbon (HC) area. a) profiles averaged over the last 46 ps of Simulation II; b) for comparison, experimental results for DOPC in number density units (figure adapted from [51]).

with experimental data. [75] report that the head groups of POPC are found to be essentially parallel to the plane of the membrane, within 30^o, while [76] report that the P–N vectors of DMPC are inclined to the bilayer plane at angles of 17^o and 27^o. [51] report an angle of 22 ± 4^o of the phosphocholine dipole with respect to the bilayer surface for DOPC in the liquid-crystal phase and [77] find 18^o for the liquid-crystal phase of DPPC. Our simulation shows that for POPC bilayers the head groups arrange in a similar fashion as previously found in experiments on DMPC and DOPC, namely tilted towards the bilayer plane, pointing into the solvent with an inclination relative to the membrane plane of about 21^o.

Two observations can be made from Fig. 20, which shows the fluctuations of the head group angle of three different lipids over the course of the simulation; (i) the large magnitude of the fluctuations of the angle of up to 78^o (lipid 64) on this short (ps) time scale, and (ii) the great variation in head group orientations as illustrated by lipids 60 and 116. Lipid 116 has its head group almost vertical to the bilayer plane during the whole simulation, while the head group of lipid 60 points inward towards the hydrocarbon region of the membrane. These findings complement experimental results which have not been able to clearly identify the range of fluctuations in the head group orientation [78].

The strong fluctuations and the wide range of possible head group angles are a major contribution to the surface roughness [79, 80], which can be observed, e.g., by atomic force microscopy [81]. The average y-position of the nitrogen atoms indicates the surface of the bilayer, and its RMS value is a measure of the surface roughness. From Simulation II we obtained an average y-position of the N atom relative to the center of the bilayer of $Y_{\rm N} = 19.08$ Å and $Y_{\rm N} = -18.87$ Å with an RMS deviation of 2.39 Å and 2.33 Å for the upper and the lower monolayer, respectively. The average length of the P–N vector was determined

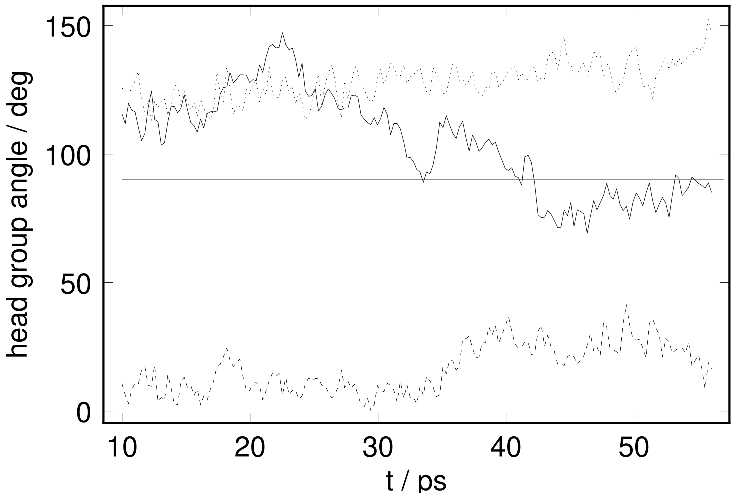

Figure 20: Fluctuations of head group orientation as given by the angle of the P–N vector with the bilayer normal. Shown are the trajectories of the head group angle for three extreme cases: lipid 64 (—) shows very strong fluctuation, lipid 116 (- - -) has its head group almost upright most of the time, and lipid 60 (....) buries its head group in the hydrocarbon region. The horizontal line indicates an angle of 90^o which corresponds to an orientation of the head group parallel to the membrane surface.

at 4.11 ± 0.001 Å, which is shorter than the 4.3 Å and 4.5 Å reported by [76] for the two molecules in the unit cell of DMPC in the crystal phase.

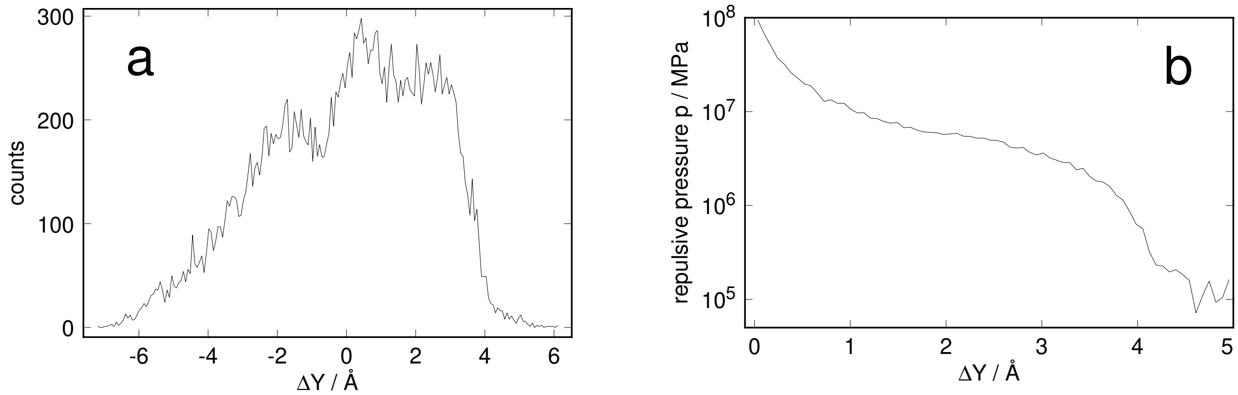

Figure 21: a) Histogram of the distance ΔY at which the nitrogen atom is found relative to the average value. Data points were sampled every 128 fs over all unrestrained lipids. The average value was calculated at each time step to allow for a possible drift of the average. 200 boxes were used to cover the range of the abscissa. b) Calculated repulsive steric protrusion pressure between two bilayers at separation ΔY if both bilayers have a distribution of protrusions as the one shown on the left side.

Fig. 21 a shows that there is a very well defined surface of the lipid bilayer about 3.5 Å away from the average position of the nitrogen atom. Within 1 Å the count of head groups per box rises from 15 to over 200.

The source of the so-called "hydration force", a strong repulsive force felt at short distances of a few Ångstrøm, between two flexible bilayers is not well understood. There is an ongoing discussion as to whether those forces are due to a structural rearrangement of water molecules close to the head groups (hydration forces) [82] or whether they are caused by steric interactions between the head groups of the two bilayers in contact (protrusion forces) [83]. It is found experimentally that the repulsion decays exponentially with the distance ΔY between the two layers, according to

$$p = Ce^{-\Delta Y/\lambda} \tag{15}$$

where the decay length λ is close to 2 Å.

[84] define the protrusion or entropic contribution to the repulsive force per unit area between two bilayers as

$$p = T\left(\frac{\partial S}{\partial \Delta Y}\right)_T \quad . \tag{16}$$

The entropy S can be expressed by the configurational integral Z as $S = k_B \ln Z$, and Z factorizes into n identical "two-particle" configurational integrals z so that $Z = z^n$. n is the number of protrusion sites per unit area ($n \approx 1/A$ with $A = 65.5\,\text{Å}^2$ as the surface area per head group, see Section "Area per Head Group") and

$$z = \int_0^{\Delta Y} dy_2 \int_{y_2}^{\Delta Y} dy_1\, \rho(y_1) \quad , \tag{17}$$

where $\rho(y)$ is the density of protrusions extending to a height y above the membrane surface. [84] did not have available any data on ρ and therefore assumed an exponential dependency $\rho(y) = \rho(y_0)e^{-y/\lambda}$. However, $\rho(y)$ can be computed from our simulation and is plotted in Fig. 21 a. For simplicity we assume the same distribution of protrusions for both approaching surfaces and we also assume that this distribution is not changed as the two surfaces approach each other. The evaluation of the configurational integrals by numberical integration is then straight forward and the protrusion contribution to the repulsive force between two POPC bilayers can be computed by numerical differentiation according to eq 16. The resulting pressure is shown in Fig. 21 b for the simulation temperature $T = 300\,\text{K}$.

The range of the obtained pressure values agrees with experimental data and other simulations. The expected exponential dependency is present in the range $\Delta Y = 1 \ldots 3\,\text{Å}$ and a fit of eq 15 yields values of $\lambda = 2.0\,\text{Å}$ and $C = 179.9\,\text{MPa}$, which are both in good agreement with experimental data [85, 86]. The more than exponential increase of the pressure for distances $\Delta Y < 1\,\text{Å}$ is in agreement with the osmotic limit [84]. The pressure values for distances of more than $\Delta Y > 4\,\text{Å}$ are unreliable because the number of data points gathered from our simulation is too small for good statistics.

Fig. 22, a ray-traced view along the negative y-axis of the top surface of the bilayer with water omitted, can be compared to images obtained with an atomic force microscope, e.g.,

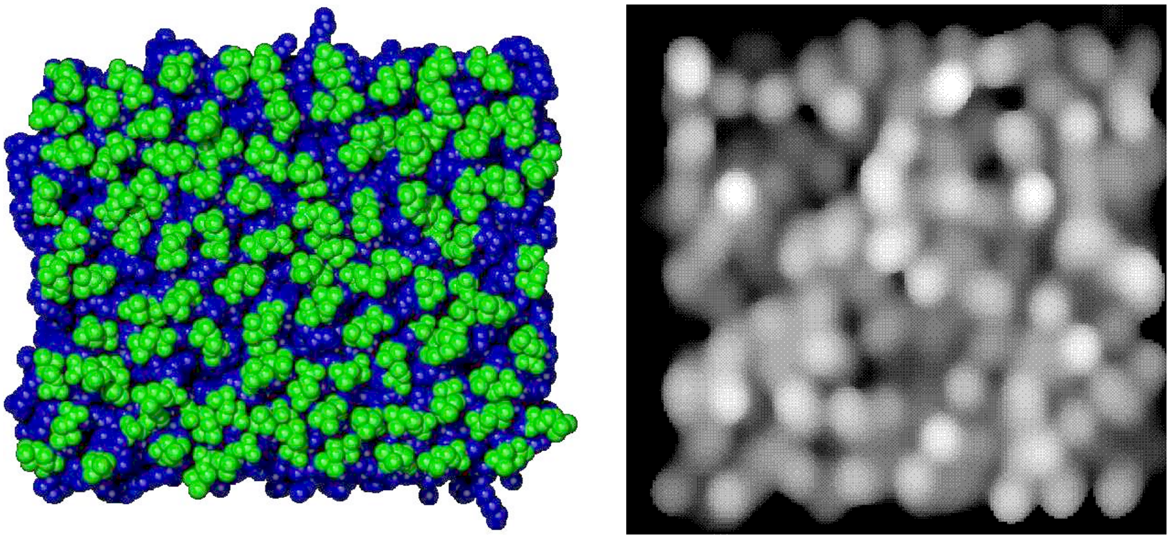

Figure 22: Surface of the upper half of the bilayer at the end of Simulation II. Left: ray-traced space filling model; the head groups are brighter colored than the backbone and the hydrocarbon part of the lipids; the water is omitted. Right: relief map; the height is grey-coded, lower points appearing darker.

Fig. 2 of [87]. The head groups are clearly visible but show a fair amount of disorder. This

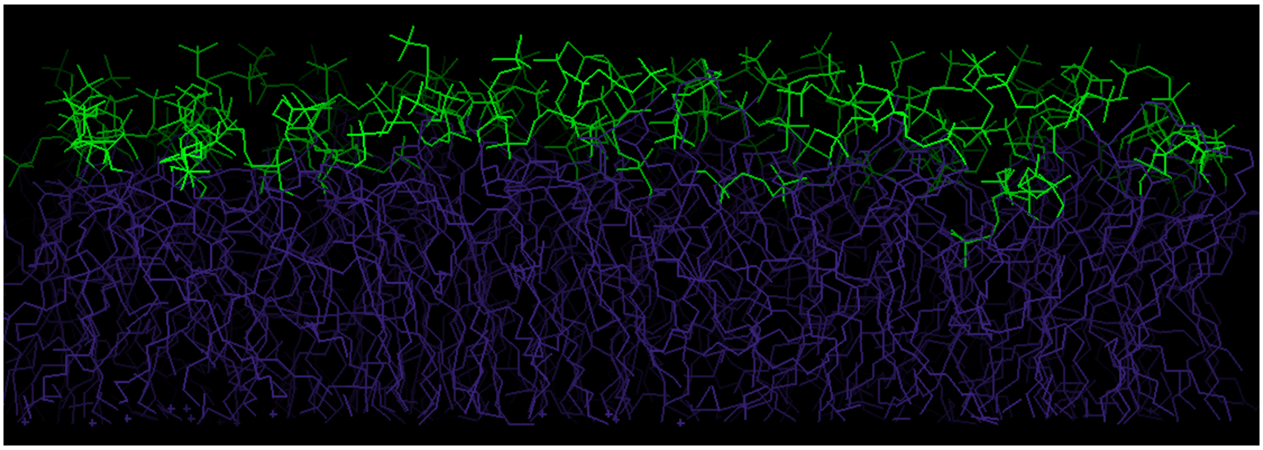

Figure 23: Side view of the upper half of the bilayer at the end of Simulation II. The head groups are brighter colored than the backbone and the hydrocarbon part of the lipids; the water is omitted for clarity.

fact is illustrated by Fig. 23, a side view of the upper monolayer. This simple line drawing allows a deep look into the layer. While most of the head groups are oriented parallel to the bilayer, some are in the upright conformation and others are burried deep in the hydrocarbon region.

Thermal Motion

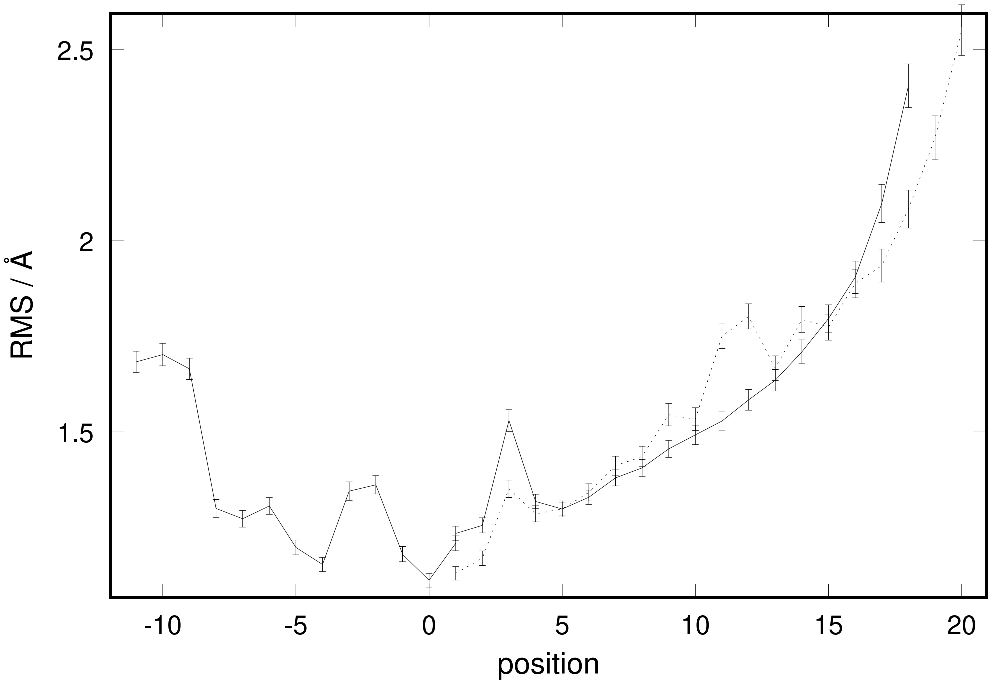

Figure 24: RMS deviation of lipid atoms from their average positions during Simulation II. The RMS values were calculated by averaging over all unrestrained lipids and using structures every 128 fs along the trajectory. The error bars indicate the standard deviation of the average. Each integer number on the abscissa corresponds to one, two, or three lipid atoms. The backbone carbons were given the numbers -1, 0, +1, starting at the sn-3 position. The headgroup atoms were assigned the numbers $-11 \ldots -1$ in the following order: the three terminal methyl carbons, N, the two methylene carbons, phosphate ester O, P, the two phosphate acid O's, and the phosphate ester O linking to the backbone. The atoms in the palmitoyl (—) and the oleoyl (.....) tails were assigned positive numbers, beginning with the ester oxygens (1), the ester carbons (2), and the carbonyl oxygens (3), and then continuing along the tails towards the terminal methyl groups, respectively.

Fig. 24 shows the RMS value of the positional fluctuations for all lipid atoms in the three sections head group, backbone, and tails. In a first step, the RMS value was computed from the last 46 ps of the trajectory for each lipid independently. Then these RMS values were averaged for each atom of the lipid over all 200 lipids and the standard deviation was computed for this averaging.

The glycerol backbone is the most rigid part of the molecule; the flexibility increases towards both ends (head and tail), but the ends of the hydrocarbon chains are by far the most flexible part. This is consistent with crystallographic measurements [88, 89], NMR results [90, 91], incoherent quasi-elastic neutron scattering [5], and joint refinement [51] which all indicate that the glycerol backbone is the most rigid portion of glycerophospholipid molecules in liquid-crystalline phospholipid bilayers. The non-chain oxygens, i.e., the carbonyl oxygens at position 3 and the oxygens of the phosphorus, positions -2 and -3 show increased flexibilities compaired to the chain, which is to be expected as they participate in only one bond.

The flexibilities of the two tails are almost identical with the remarkable exception of the double bonded carbon atoms (positions 11 and 12 in Fig. 24) which show an increased RMS value compared to the saturated sn-1 chain (we will refer to this increase as the "C=C-effect"). The increased flexibility is confirmed by experiments [51]. However, the explanation given by Wiener and White, namely that this is due to the fact that the hydrocarbon tails are tethered at both ends by the carbonyls and terminal methyls repectively, must be rejected, as otherwise this increase in mobility should appear in both chains. Our simulation data, which allow for direct comparison between the saturated and unsaturated tails, show clearly that the C=C-effect is due to the unsaturation, as the increase in thermal mobility associated with the double bond is absent in the fully saturated chain (see Fig. 24). Furthermore, the steady increase in thermal mobility towards the ends of the chains seen in our simulation is not in accordance with the idea of a tether restricting the motion of the terminal methyls.

From Fig. 24 alone it is not clear whether the C=C-effect is a cooperative effect only present in aggregates of multiple lipids, or a geometric effect of the *cis*-bond which would then also manifest itself in a simulation of a single lipid. An estimate of the necessary simulation time for a single lipid simulation can be obtained as follows. The C=C-effect was observed if the RMS values were computed from trajectories of 5 ps or longer. It did not appear if only a 1 ps trajectory was used for the computation of the RMS values. The effect was also absent if the final averaging over all 200 lipids was omitted and instead the RMS values (of a 46 ps trajectory) of a single lipid were plotted. This leads to an estimate of $200 \cdot 5\,\mathrm{ps} = 10\,\mathrm{ns}$ simulation time necessary for a single lipid simulation. We have performed such a 10 ns molecular dynamics simulation of one lipid in vacuum (unpublished results). As there was no distinctive increase in the RMS values of the double bonded C atoms compared to the single bonded atoms at the same position in the other chain, one can conclude that the C=C-effect is a cooperative phenomenon caused by the interactions of several lipids in a bilayer.

Final Structure

Ray traced images of the final structures of Simulation I and II are presented in Fig. 25. In both images the thin layer of restrained water (red) which prevents disintegration of the assemblies and assures their structural stability is visible. It can also be seen that there is ample free water (orange) between the boundary and the lipids to ensure that the influence of the boundary on the lipids is small. The reduction in thickness of the bilayer after the gel to liquid-crystal phase transition is clearly visible. The most striking difference, perhaps, is the decrease in order of the hydrocarbon tails from the gel to the liquid-crystal phase. The different shape of the watercaps (ellipsoid in Simulation I and flat in Simulation II) is a technicality (see Methods) and has no influence on the behavior of the bilayer.

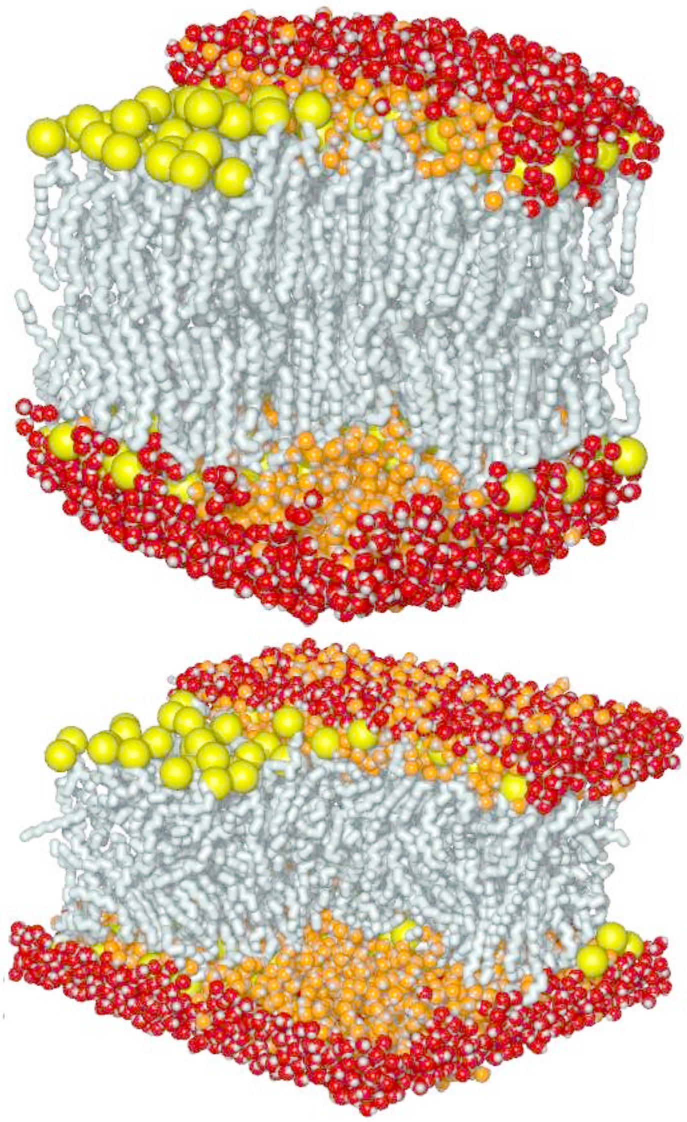

Figure 25: Final membrane structures resulting from Simulation I (gel phase, top) and Simulation II (liquid-crystal phase, bottom) of the POPC bilayer. A fraction of the water and the lipid molecules has been omitted to provide a view of the core of the membranes; grey: hydrocarbon tails; yellow spheres: head groups; red: restrained water molecules; orange: unrestrained water molecules.

Discussion

In this paper we have presented the structure of a simulated patch of membrane of 200 lipid molecules with a size of 85 Å × 100 Å. This size is large enough to permit the addition of various biomolecules such as drugs, transmembrane proteins (e.g., bacteriorhodopsin [4], porin [92] or the photosynthetic reaction centers [93, 94]), or proteins interacting with membranes (e.g., phospholipase A2 [95] or annexins [96]). The simulation included all atoms explicitly, except non-polar hydrogen atoms, and described forces according to a conventional molecular dynamics force field. In order to account properly for trans-membrane Coulomb interactions between head groups on opposite sides of the bilayer, long-range interactions were not cut-off. The volume simulated has been controlled by adjusting a stochastic boundary; this allowed control of the area per lipid, the quantity which determines the various phases of a membrane. Area per lipid values have been adjusted for two different membrane phases, the highly ordered gel phase and the less ordered liquid-crystal phase, the latter being assumed to constitute the native state of the membrane in biological cells. The computations for the respective molecular dynamics simulations consumed a total of 20 months of processor time on a machine of Cray 2 like processor power. This extraordinary effort was undertaken because it was expected that the membrane patch described will serve as a building block for numerous later investigations of the interactions of biopolymers with membranes, one of the most important issues in understanding the molecular biology of the cell[7].

A first step towards studying heterogeneous membrane assemblies requires that one verifies that the membrane model used does indeed show the properties of actual biological membranes. We have therefore presented in this paper evidence that the simulated membrane patch, in many respects, shows good agreement with observations. We employed for this purpose all properties that can be determined from molecular dynamics simulations lasting about 100 ps and for which data exist in the literature. Key characteristics determined are the deuterium order parameter profiles and RMS fluctuations along the lipid chains, the spatial distribution of lipid segments and water, the head group angles relative to the membrane normal, the pressure in the membrane, the lateral diffusion constant governing random motion over about 100 ps, and the repulsive steric protrusion pressure [84]. Close agreement with observations provides justification for the use of the membrane structure provided here for further studies of protein–membrane interactions. However, we certainly recognize and advocate the need for improvement of the membrane model provided here. The key shortcomings are the limitation in simulation time (a total of 263 ps thus far) and the relatively small size of the membrane and the water layer, compared to biological cell dimensions. Improvements in these respects will yield better structures as well as better statistics for comparison with membrane data.

Most other simulations of membranes carried out so far dealt with smaller size systems, or did not describe the system at the level of detail common to molecular dynamics methods, i.e., a level required to add biopolymers like drugs and proteins to describe the resulting interactions through molecular dynamics simulations. In the present simulations, as opposed to most previous simulations, we opted for use of a stochastic boundary rather than periodic boundary conditions because the stochastic boundary allows one to directly control the area per lipid molecule. The primary reason against the employment of periodic boundary conditions has been the difficulty of describing Coulomb interactions properly for such systems. The importance of transmembrane Coulomb forces between head groups prevents the use of

[7]The membrane structure can be made available to other researchers as a pdb file by contacting the first author.

small cut-off ranges; on the other hand, suitable methods to carry out Ewald summations for a planar lattice of very large (26,000 atoms) elementary cells are not currently available. However, we expect that once satisfactory structures of membrane patches in the various states of the membrane (i.e., gel, liquid crystal, etc.) exist, such structures can serve as building blocks for an array of patches treated as many identical copies in a plane.

There are many important aspects of membrane structure and dynamics other than the ones considered here, for example: the determination of rotational motions and of correlations in the motions of lipids; the hopping of lipids which should require minimal simulation times in the order of (area per head group) / (self-diffusion coefficient of lipids) $\approx$ 100 ns; the detailed description of tail dynamics such as the distribution of trans/gauche bonds and kinks; a demonstration of the existence of crankshaft motions in the tail; a test of anisotropies of the motion of lipid segments; the interdigitation of lipids at the hydrocarbon core; the determination of the surface potential of model membranes; the influence of applied electric fields, e.g., on the head group orientation; the tilt angle of lipid molecules; the possible occurrence of networks of hydrogen bonds in the head group region; an analysis of bond vibrations and a normal mode analysis of lipid vibrational motions in bilayers; radial distribution functions (hydration shells) of water around different lipid atoms; analysis of the property of the water layer near membranes; more extensive characterizations of the gel and liquid-crystal phases; the comparison of membrane structures for different lipid compositions. Obviously, there exists an enormous research agenda for simulations of model membranes defined through many years of experimental work.

Therefore, we want finally to comment on the computational technology which will pave the way for molecular dynamics simulations of biological membranes. In this respect it is important to note that the present molecular dynamics study of the structure of lipid bilayers is probably the first instance of an investigation which required the technology of massively parallel computing. Much as the advent of supercomputers in the eighties opened an avenue for computational studies of biopolymers, the advent of massively parallel computers opens the possibility of computational investigations of molecular aggregates encompassing several tens of thousands of atoms. We have not emphasized in the present article the corresponding issues regarding the architecture of the parallel computer employed and the organization of computational and communication tasks across the computer since this had been described previously [29, 39, 41, 40].

The simulations reported here were carried out during the past three years on a 60 node computer designed and built in 1988 which achieved the same sustained performance during the molecular dynamics simulations as a Cray 2 processor. More recent models of parallel machines provide a speed increase of about a factor of ten or more and improvements in node–node communication allow the cooperation of ten times more processors. An efficient scheme for evaluation of Coulomb forces using a parallel implementation of the Fast Multipole Algorithm (FMA, [97, 98, 99, 35]) should yield another factor of ten in speed up compared with the program presently used by us[8]. Hence, one can expect that within a year the sim-

[8]It must be pointed out in this respect that we have employed in the reported simulations the so-called distance class algorithm [1] which yields an improvement on the order of ten compared to the straight forward

ulations carried out by us over a time span of 20 months of uninterrupted computer time can be completed within a day. This perspective underscores that simulations of biological membranes and their integral proteins will soon be carried out routinely. The important role of membranes in biological cells will certainly provide a strong motivation for such studies. It is more difficult to predict in how far respective investigations will be impeded through lack of structural information of relevant proteins, but even given the present knowledge of protein structures (bacteriorhodopsin, the photosynthetic reaction centers, porin, phospholipase, annexins) exciting opportunities for future studies exist.

Acknowledgements

Participation of HH in the CECAM workshop "Molecular Dynamics Simulations of Proteins in Lipid Membranes" at the University of Paris at Orsay, January 1992, has contributed significantly to the perspectives set forth in this article. We thank Andreas Windemuth for stimulating discussions and rendering of Fig. 25 and Barbara Napier for rendering of Figs. 1 and 10 and help with other illustrations.

References

[1] Grubmüller, H.; Heller, H.; Windemuth, A., and Schulten, K. *Molecular Simulation*, 1991, 6, 121.

[2] Büldt, G.; Gally, H. U.; Seelig, A.; Seelig, J., and Zaccai, G. *Nature*, 1978, 271, 182.

[3] Pak, J. H.; Bork, V. P.; Norberg, R. E.; Creer, M. H.; Wolf, R. A., and Gross, R. W. *Biochemistry*, 1987, 26, 4824.

[4] Henderson, R.; Baldwin, J.; Ceska, T.; Zemlin, F.; Beckmann, E., and Downing, K. *J. Mol. Biol.*, 1990, 213, 899.

[5] König, S.; Pfeiffer, W.; Bayerl, T.; Richter, D., and Sackmann, E. *J. Phys. II France*, August 1992, 2, 1589.

[6] Marčelja, S. *Nature*, February 1973, 241, 451.

[7] Silver, B. L. *The Physical Chemistry of Membranes: an Introduction to the Structure and Dynamics of Biological Membranes*, Allen & Unwin and The Solomon Press: Publisher Creative Services Inc., Jamaica, New York, 1985.

[8] Cevc, G. and Marsh, D. *Phospholipid Bilayers: Physical Principles and Models*, John Wiley & Sons: New York, 1987.

[9] Gennis, R. B. *Biomembranes: Molecular Structure and Function*, Springer-Verlag: New York, 1989.

[10] Pastor, R. W.; Venable, R. M., and Karplus, M. *Proc. Natl. Acad. Sci. USA*, February 1991, 88, 892.

---

summation over N^2 pairs.

[11] Schwyzer, R. *Biopolymers*, 1991, 31, 785.

[12] McCammon, J. A.; Gelin, B. R., and Karplus, M. *Nature*, June 1977, 267, 585.

[13] Levitt, M. *J. Mol. Biol.*, 1983, 168, 595.

[14] Karplus, M. and McCammon, J. A. *Ann. Rev. Biochem.*, 1983, 53, 263.

[15] Brooks III, C. L.; Karplus, M., and Pettitt, B. M. *Proteins: A Theoretical Perspective of Dynamics, Structure and Thermodynamics*, John Wiley & Sons: New York, 1988.

[16] Edholm, O. and Johansson, J. *Eur. Biophys. J.*, 1987, 14, 203.

[17] Levitt, M. and Sharon, R. *Proc. Natl. Acad. Sci. USA*, 1988, 85, 7557.

[18] Warshel, A. Electrostatic free energy as the fundamental structure function correlator in proteins: Some perspectives from microscopic simulations of proteins functions. In Rivail, J.-L., ed., *Modelling of Molecular Structures and Properties*, volume 71 of *Studies in Physical and Theoretical Chemistry*, 515, Amsterdam, 1990. Elsevier Science Publishers.

[19] Michelangeli, F.; Grimes, E. A.; East, J. M., and Lee, A. G. *Biochemistry*, 1991, 30, 342.

[20] Ploeg, P. v. d. and Berendsen, H. J. C. *J. Chem. Phys.*, March 1982, 76, 3271.

[21] Ploeg, P. v. d. and Berendsen, H. J. C. *Mol. Phys.*, 1983, 49, 233.

[22] Damodaran, K. V.; Merz, K. M., Jr., and Gaber, B. P. *Biochemistry*, 1992, 31, 7656.

[23] Egberts, E. and Berendsen, H. J. C. *J. Chem. Phys.*, September 1988, 89, 3718.

[24] Watanabe, K.; Ferrario, M., and Klein, M. L. *J. Phys. Chem.*, 1988, 92, 819.

[25] Wendoloski, J. J.; Kimatian, S. J.; Schutt, C. E., and Salemme, F. R. *Science*, 1989, 243, 636.

[26] Pastor, R. W.; Venable, R. M., and Karplus, M. *J. Chem. Phys.*, 1988, 89, 1112.

[27] Pastor, R. W.; Venable, R. M.; Karplus, M., and Szabo, A. *J. Chem. Phys.*, July 1988, 89, 1128.

[28] Loof, H. d.; Harvey, S. C.; Segrest, J. P., and Pastor, R. W. *Biochemistry*, 1991, 30, 2099.

[29] Heller, H.; Grubmüller, H., and Schulten, K. *Molecular Simulation*, 1990, 5, 133.

[30] Windemuth, A. and Schulten, K. *Molecular Simulation*, 1991, 5, 353.

[31] Beeman, D. *J. Comput. Phys.*, 1976, 20, 130.

[32] Streett, W. B.; Tildesley, D. J., and Saville, G. *Mol. Phys.*, 1978, 35, 639.

[33] Greengard, L. and Rohklin, V. *J. Comp. Phys.*, 1987, 73, 325.

[34] Board, J. A., Jr.; Batchelor, R. R., and Leathrum, J. F., Jr. High performance implementations of the fast multipole algorithm. In *Symposium on Parallel and Vector Computation in Heat Transfer, Proc. 1990 AIAA/ASME Thermophysics and Heat Transfer Conference*, 1990.

[35] Board, J. A., Jr.; Causey, J. W.; Leathrum, J. F., Jr.; Windemuth, A., and Schulten, K. *Chem. Phys. Lett.*, 1992, 89.

[36] Wiener, M. C. and White, S. H. *Biophys. J.*, 1991, 59, 162.

[37] Lafleur, M.; Cullis, P. R., and Bloom, M. *Eur. Biophys. J.*, 1990, 19, 55.

[38] Nagle, J. F. and Wiener, M. C. *Biochim. Biophys. Acta*, 1988, 942, 1.

[39] Boehncke, K.; Heller, H.; Grubmüller, H., and Schulten, K. Molecular dynamics simulations on a systolic ring of transputers. In Wagner, A. S., ed., *NATUG 3: Transputer Research and Applications 3*, 83, Amsterdam, 1990. North American Transputer Users Group, IOS Press.

[40] Heller, H. and Schulten, K. *Chemical Design Automation News (CDA News)*, August 1992, 7, 11.

[41] Sinha, A. B.; Schulten, K., and Heller, H. *Comput. Phys. Commun.*, 1994, 78, 265.

[42] Heller, H. Dynamiksimulation sehr großer Makromoleküle am Beispiel des photosynthetischen Reaktionszentrums von Rhodopseudomonas viridis. Diploma thesis, Technical University of Munich, Physics Department, T 30, James-Franck-Street, D-8046 Garching / Munich, 1988.

[43] Banko, B. and Heller, H. *User Manual for EGO — Release 1.1*, 1991. [Beckman Institute Technical Report TB-92-07].

[44] Brooks, B. R.; Bruccoleri, R. E.; Olafson, B. D.; States, D. J.; Swaminathan, S., and Karplus, M. *J. Comp. Chem*, 1983, 4, 187.

[45] Brünger, A. T. *X-PLOR*. The Howard Hughes Medical Institute and Department of Molecular Biophysics and Biochemistry, Yale University, New Haven, CT, May 1988.

[46] Brünger, A. T. *X-PLOR, Version 2.1.* The Howard Hughes Medical Institute and Department of Molecular Biophysics and Biochemistry, Yale University, 260 Whitney Avenue, P.O. Box 6666, New Haven, CT 06511, 1990.

[47] Verlet, L. *Phys. Rev.*, July 1967, 159, 98.

[48] Ryckaert, J.-P.; Ciccotti, G., and Berendsen, H. J. C. *J. Comp. Phys.*, 1977, 23, 327.

[49] Raine, A. R. C. Molecular dynamics simulation of proteins on an array of transputers. In Pritchard, D. J. and Scott, C. J., eds., *Applications of Transputers 2., Proccedings of the Second International Conference on Applications of Transputers*, 272, Amsterdam, Netherlands, 1990. IOS Press.

[50] Polygen Corporation, 200 Fifth Av., Waltham, MA 02254, U.S.A. *Quanta*, 1988.

[51] Wiener, M. C. and White, S. H. *Biophys. J.*, February 1992, 61, 434.

[52] Jorgensen, W. L.; Chandrasekhar, J.; Madura, J. D.; Impey, R. W., and Klein, M. L. *J. Chem. Phys.*, 1983, 79, 926.

[53] Schlenkrich, M.; MacKerell, A. D., Jr., and Karplus, M. in preparation, 1992.

[54] Berkowitz, M. and McCammon, J. A. *Chem. Phys. Lett.*, July 30 1982, 90, 215.

[55] Brooks III, C. L.; Brünger, A., and Karplus, M. *Biopolymers*, 1985, 24, 843.

[56] Brünger, A. T.; Brooks III, C. L., and Karplus, M. *Chem. Phys. Lett.*, March 1984, 105, 495.

[57] Berendsen, H. J. C.; Postma, J. P. M.; Gunsteren, W. F. v.; DiNola, A., and Haak, J. R. *J. Chem. Phys.*, 1984, 81, 3684.

[58] *CRC, Handbook of Chemistry and Physics*, CRC Press Inc.: Cleveland, Ohio, 1975.

[59] Beveridge, D. L. and DiCapua, F. M. *Ann. Rev. Biophys. Biophys. Chem.*, 1989, 18, 431.

[60] Seelig, J. and Waespe-Šarčevič, N. *Biochemistry*, 1978, 17, 3310.

[61] Nadler, W.; Tavan, P., and Schulten, K. *Eur. Biophys. J.*, 1985, 12, 25.

[62] Berendsen, H. J. C. and Gunsteren, W. F. v. Practical algorithms for dynamic simulations. In Ciccotti, G. C. and Hoover, W. G., eds., *Proceedings of the International School of Physics, "Enrico Fermi"*, volume on course 97, 43, Amsterdam, 1986. North-Holland.

[63] König, S. *Untersuchungen zur molekularen Bewegung und Diffusion von Membranen mittels inkohärenter, quasielastischer Neutronenstreuung und Deuterium-NMR*. PhD thesis, Technical University of Munich, 1993.

[64] Seelig, A. and Seelig, J. *Biochemistry*, 1977, 16, 45.

[65] Seelig, J. and Seelig, A. *Quart. Rev. Biophys.*, 1980, 13, 19.

[66] Seelig, J. *Quart. Rev. Biophys.*, 1977, 10, 353.

[67] Galla, H.-J.; Hartmann, W.; Theilen, U., and Sackmann, E. *J. Membr. Biol.*, 1979, 48, 215.

[68] Pfeiffer, W.; Henkel, T.; Sackmann, E.; Knoll, W., and Richter, D. *Europhys. Lett.*, January 15 1989, 8, 201.

[69] Cohen, M. H. and Turnbull, D. *J. Chem. Phys.*, 1959, 31, 1164.

[70] Rand, R. P. and Parsegian, V. A. *Biochim. Biophys. Acta*, 1989, 988, 351.

[71] Wiener, M. C. and White, S. H. *Biophys. J.*, February 1992, 61, 428.

[72] Seelig, A. and Seelig, J. *Biochemistry*, 1974, 13, 4839.

[73] Schindler, H. and Seelig, J. *Biochemistry*, June 3 1975, 14, 2283.

[74] Seelig, J. and Browning, J. L. *FEBS Lett.*, August 1978, 92, 41.

[75] Seelig, J.; Macdonald, P. M., and Scherer, P. G. *Biochemistry*, December 1 1987, 26, 7534.

[76] Pearson, R. H. and Pascher, I. *Nature*, 1979, 281, 499.

[77] Akutsu, H. and Nagamori, T. *Biochemistry*, 1991, 30, 4510.

[78] Büldt, G.; Gally, H. U.; Seelig, J., and Zaccai, G. *J. Mol. Biol.*, 1979, 134, 673.

[79] Owenson, B. and Pratt, L. R. *J. Phys. Chem.*, 1984, 88, 6048.

[80] Northrup, S. H. and Curvin, M. S. *J. Phys. Chem.*, 1985, 89, 4707.

[81] Egger, M.; Ohnesorge, F.; Weisenhorn, A. L.; Heyn, S. P.; Drake, B.; Prater, C. B.; Gould, S. A. C.; Hansma, P. K., and Gaub, H. E. *J. Struct. Biol.*, 1990, 103, 89.

[82] Marčelja, S. and Radic, N. *Chem. Phys. Lett.*, August 15 1976, 42, 129.

[83] Israelachvili, J. N. and Wennerström, H. *Langmuir*, 1990, 6, 873.

[84] Israelachvili, J. N. and Wennerström, H. *J. Phys. Chem.*, 1992, 96, 520.

[85] McIntosh, T. J. and Simon, S. A. *Biochemistry*, 1986, 25, 4058.

[86] McIntosh, T. J.; Magid, A. D., and Simon, S. A. *Biochemistry*, 1989, 28, 7904.

[87] Radmacher, M.; Tillmann, R. W.; Fritz, M., and Gaub, H. E. *Science*, September 25 1992, 257, 1900.

[88] Hitchcock, P. B.; Mason, R.; Thomas, K. M., and Shipley, G. G. *Proc. Natl. Acad. Sci. USA*, 1974, 71, 3036.

[89] Elder, M.; Hitchcock, P.; Mason, R., and Shipley, G. G. *Proc. R. Soc. Lond. A. (Math. Phys. Sci.)*, 1977, 354, 157.

[90] Strenk, M. L.; Westerman, P. W., and Doane, J. W. *Biophys. J.*, 1985, 48, 765.

[91] Braach-Maksvytis, V. L. B. and Cornell, B. A. *Biophys. J.*, 1988, 53, 839.

[92] Garavito, R. M.; Jenkins, J.; Jansonius, J. N.; Karlson, R., and Rosenbusch, J. P. *J. Mol. Biol.*, 1983, 164, 313.

[93] Deisenhofer, J. and Michel, H. *The crystal structure of the photosynthetic reaction center from Rhodopseudomonas viridis*, Plenum Press: London, 1987, volume 149 of *The photosynthetic bacterial reaction center: Structure and dynamics*.

[94] Michel, H. and Deisenhofer, J. *Chemica Scripta*, November 1987, 27B, 173.

[95] Dijkstra, B. W.; Kalk, K. H.; Hol, W. J. H., and Drenth, J. *J. Mol. Biol.*, 1983, 147, 97.

[96] Creutz, C. E. *Science*, November 6 1992, 258, 924.

[97] Greengard, L. and Gropp, W. D. A parallel version of the fast multipole method. Technical report, Rept. YALEU/DCS/RR-640, 1988.

[98] Board, J. A., Jr. and Leathrum, J. F., Jr. The fast multipole algorithm on transputer networks. In Wagner, A. S., ed., *Transputer Research and Applications 3, NATUG-3 Proceedings*, 63, Amsterdam, 1990. The North American Transputer Users Group, IOS Press.

[99] Leathrum, J. F., Jr. and Board, J. A., Jr. Parallelization of the fast multipole algorithm using the B012 transputer network. In Stiles, D.; Kunii, T. L., and Bakkers, A., eds., *TRANSPUTING '91*, volume 1, 296, Amsterdam, April 1991. IOS Press.

A Simulation Parameters

atom	$q\,/\,e$	$\varepsilon\,/\,(\frac{\text{kcal}}{\text{mol}})$	$\sigma\,/\,\text{Å}$	$\varepsilon_{1:4}\,/\,(\frac{\text{kcal}}{\text{mol}})$	$\sigma_{1:4}\,/\,\text{Å}$
C351	0.40	0.1811	3.8576	0.1000	3.3854
C352	0.40	0.1811	3.8576	0.1000	3.3854
C353	0.40	0.1811	3.8576	0.1000	3.3854
N35	−0.60	0.2384	2.8510	0.2384	2.8510
C34	0.40	0.1142	3.9823	0.1000	3.3854
C33	0.10	0.1142	3.9823	0.1000	3.3854
O32	−0.55	0.1591	2.8509	0.1591	2.8509
P31	1.50	0.0903	3.2070	0.0903	3.2070
O311	−0.80	0.6469	2.8509	0.6469	2.8509
O312	−0.80	0.6469	2.8509	0.6469	2.8509
O3	−0.55	0.1591	2.8509	0.1591	2.8509
C3	0.10	0.1142	3.9823	0.1000	3.3854
C2	0.13	0.0486	4.2140	0.1000	3.3854
O2	−0.34	0.1591	2.8509	0.1591	2.8509
C1	0.13	0.1142	3.9823	0.1000	3.3854
O1	−0.34	0.1591	2.8509	0.1591	2.8509
O101	−0.52	0.1591	2.8509	0.1591	2.8509
C101	0.63	0.1200	3.7418	0.1000	3.3854
C102	0.10	0.1142	3.9823	0.1000	3.3854
C103	0.00	0.1142	3.9823	0.1000	3.3854
C104	0.00	0.1142	3.9823	0.1000	3.3854
C105	0.00	0.1142	3.9823	0.1000	3.3854
C106	0.00	0.1142	3.9823	0.1000	3.3854
C107	0.00	0.1142	3.9823	0.1000	3.3854
C108	0.00	0.1142	3.9823	0.1000	3.3854
C109	0.00	0.1142	3.9823	0.1000	3.3854
C110	0.00	0.1142	3.9823	0.1000	3.3854
C111	0.00	0.1142	3.9823	0.1000	3.3854
C112	0.00	0.1142	3.9823	0.1000	3.3854
C113	0.00	0.1142	3.9823	0.1000	3.3854
C114	0.00	0.1142	3.9823	0.1000	3.3854
C115	0.00	0.1142	3.9823	0.1000	3.3854
C116	0.00	0.1811	3.8576	0.1000	3.3854
O201	−0.52	0.1591	2.8509	0.1591	2.8509
C201	0.63	0.1200	3.7418	0.1000	3.3854
C202	0.10	0.1142	3.9823	0.1000	3.3854
C203	0.00	0.1142	3.9823	0.1000	3.3854
C204	0.00	0.1142	3.9823	0.1000	3.3854
C205	0.00	0.1142	3.9823	0.1000	3.3854
C206	0.00	0.1142	3.9823	0.1000	3.3854
C207	0.00	0.1142	3.9823	0.1000	3.3854
C208	0.00	0.1142	3.9823	0.1000	3.3854
C209	0.00	0.0903	3.2070	0.0903	3.2070
C210	0.00	0.0903	3.2070	0.0903	3.2070
C211	0.00	0.1142	3.9823	0.1000	3.3854
C212	0.00	0.1142	3.9823	0.1000	3.3854
C213	0.00	0.1142	3.9823	0.1000	3.3854
C214	0.00	0.1142	3.9823	0.1000	3.3854
C215	0.00	0.1142	3.9823	0.1000	3.3854
C216	0.00	0.1142	3.9823	0.1000	3.3854
C217	0.00	0.1142	3.9823	0.1000	3.3854
C218	0.00	0.1811	3.8576	0.1000	3.3854

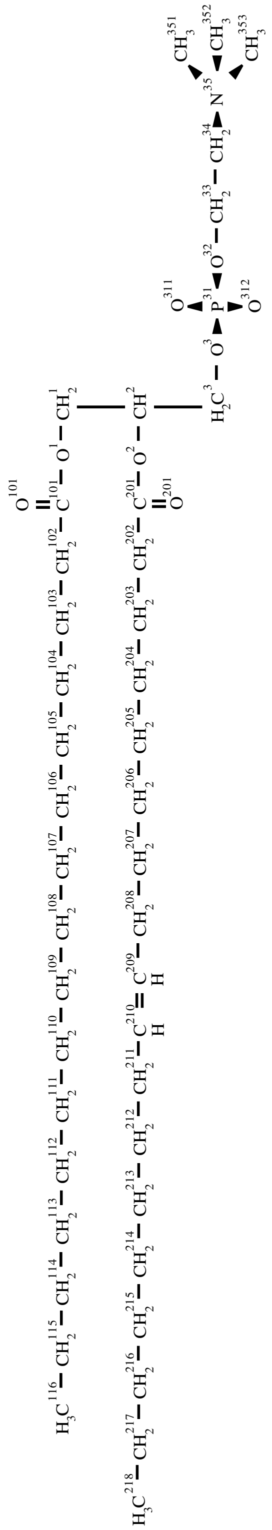

Simulation parameters used for Simulation II. The charges have been taken from the parameter file of Charmm22 [53], while the van der Waals parameters have been taken from the X-PLOR parameter file `param19.pro` [46] and from *ChemNote* (within *Quanta* [50]).